and cloned into the pCMMP retrovirus vector (30). In this vector, the T7 RNApol gene is followed by an internal ribosome entry site and a GFP gene.

Cells and antibodies. COS7 cells, 293 cells, and MAGI cells were grown in Dulbecco's modified essential medium (DMEM; Sigma, St. Louis, Mo.) supplemented with 10% fetal bovine serum (FBS) (HyClone Laboratories, Logan, Utah) and penicillin-streptomycin (Gibco-BRL, Rockville, Md.). MAGI cells were grown in DMEM supplemented with 10% FBS, penicillin-streptomycin, Geneticine (0.2 mg/ml), and hygromycin B (0.1 mg/ml) (16). Jurkat cells and H9 cells were grown in RPMI 1640 (Sigma) supplemented with 10% FBS and penicillin-streptomycin. Cells were kept under conditions of 5% CO_2 in a humidified incubator. OKT4 is an anti-CD4 monoclonal antibody and was obtained from Ortho Diagnostic System (Raritan, N.J.). Anti-gp120 polyclonal antibody was obtained from Fitzgerald Industries International, Inc. (Concord, Mass.). The purified anti-gp120 monoclonal antibody prepared from hybridoma 902 was kindly provided by Y. Yokota of the National Institute of Infectious Diseases, Tokyo, Japan. Hybridoma 902 was obtained from Bruce Chesebro through the AIDS Research and Reference Reagent Program, Division of AIDS, National Institute of Allergy and Infectious Diseases, National Institutes of Health (7, 33). 293CD4 cells were isolated from 293 cells that had been transfected with pMACS 4-IRESII (Miltenyi Biotec GmbH, Bergisch Gladbach, Germany) by use of a MACSelect4.2 system (Miltenyi Biotec GmbH). Serum from a patient infected with HIV-1 was kindly provided by T. H. Lee of Harvard School of Public Health, Boston, Mass.

Protein analysis. The WT and mutant HXB2RU3ΔN constructs were transfected into COS7 cells by the use of Gene Pulsar II (Bio-Rad, Hercules, Calif.). In brief, COS7 cells were suspended in serum-free DMEM and electroporated with 4 μg of proviral DNA at a setting of 250 kV and 950 μF. At 72 h after transfection, cell and virus lysates were prepared for protein analysis. Transfected COS7 cells were collected by scraping and were centrifuged (Allegra 6KR system; Beckman Coulter, Fullerton, Calif.) at 2,000 × *g* for 10 min. The cell pellets were dissolved in radioimmunoprecipitation assay lysis buffer (0.05 M Tris-Cl [pH 7.2] including 0.15 M NaCl, 1% Triton X-100, 1% sodium deoxycholate, and 0.1% sodium dodecyl sulfate [SDS]) and centrifuged (Himac CS 120fx system; Hitachi, Tokyo, Japan) at 314,000 × *g* for 45 min at 4°C. The supernatants were subjected to SDS-polyacrylamide gel electrophoresis (PAGE). To analyze viral proteins, the supernatants from culture media were spun (Allegra 6KR system) (2,000 × *g* for 20 min) to clear cell debris, filtered through 0.45-μm-pore-size filters (Millipore, Bedford, Mass.), and then centrifuged (SW28 rotor; Beckman Coulter) at 4°C for 1.5 h on 3 ml of a 20% sucrose cushion at 113,000 × *g*. Virus pellets were dissolved in radioimmunoprecipitation assay lysis buffer for protein analysis by SDS-PAGE. Cell and virus lysates were run on an SDS polyacrylamide gel (DRC, Tokyo, Japan) (7.5 to 15% gradient), and proteins were blotted onto Immobilon-P (Millipore) by passive transfer as described previously (21). The immunoblotting procedure was as follows. Before addition of the serum or monoclonal antibodies, the membranes were blocked with 3% bovine serum albumin (Sigma) dissolved in 0.2% Tween 20–PBS at room temperature for 30 min. Enhanced chemiluminescence (Roche Molecular Biochemicals, Mannheim, Germany) and a lumi-imager (Roche) were used to detect the bands after probing with the patient serum or with anti-gp120 polyclonal antibody. Anti-human- and anti-goat-sheep immunoglobulin G-biotin conjugates and streptavidin-horseradish peroxidase were purchased from Amersham Biosciences UK Limited (Buckinghamshire, United Kingdom).

MAGI cell assay. MAGI cells were cultured in a 96-well plate for 48 h and then transfected with 0.25 μg of proviral DNA by FuGene6 (Roche Molecular Biochemicals). At 48 after transfection, the transfected MAGI cells were fixed using PBS containing 0.5% glutaraldehyde and were stained for β-galactosidase as described previously (16). The nuclei in multinucleated cells were counted. Five randomly selected fields were evaluated for each mutant.

Infection study. For the infection study, the virus seed was prepared by transfecting 1 μg of the proviral DNA into 10^6 of COS7 cells by FuGene6. At 72 h after transfection, the culture supernatant was filtered through 0.45-μm-pore-size filters (Millipore) and the p24 amount was determined using a p24 enzyme-linked immunosorbent assay (ELISA). Jurkat cells were infected with each virus adjusted by the p24 amount (10 ng of p24 per 10^6 cells to be infected). The infection was monitored by measuring the p24 amount of the culture supernatant at the indicated time point after infection. A p24 ELISA was performed using a p24 RETRO-TEK ELISA kit (ZeptoMetrix, Buffalo, N.Y.).

Flow cytometry. At 48 after transfection by FuGene6, the COS7 cells that had been transfected with each Env expression vector (pElucEnv WT, MSD GpA, MSD GpAG831, MSD VSV-G, or EnvKO) were stained with the 902 monoclonal antibody for 1 h at 4°C (10 μg/ml in PBS with 2% FBS), incubated with biotin-XX goat anti-mouse immunoglobulin G (Molecular Probes, Eugene, Oreg.) for 30 min at 4°C, and then treated with streptavidin Alexa Fluor 555 (Molecular Probes) for 30 min at 4°C and finally fixed with 1% paraformaldehyde in PBS. Cells were suspended in PBS with 2% FBS and analyzed with Becton Dickinson FACSCalibur and CellQuest software (BD Biosciences Immunocytometry Systems, San Jose, Calif.). A double gate was defined by forward versus side scatter and by the amount of GFP (FL-1). A total of 10,000 events within this gate were collected for analysis.

CD4-binding assay. To evaluate the CD4-binding capacity of each MSD-mutant Env, cell lysates prepared from the COS7 cells transfected with each Env expression vector (pElucEnv WT, MSD GpA, MSD GpAG831, or MSD VSV-G) and a CD4 expression vector by FuGene6 were prepared. At 72 h after transfection, the transfected COS7 cells were suspended in 250 μl of a binding buffer, 0.5% Triton X-100 in PBS, supplied with the Complete protease-inhibitor cocktail (Roche Molecular Biochemicals). Aliquots of 50 μl from each lysate were mixed together, and 2 μl of OKT-4 and 5 μl of protein G Magnetic Beads (New England BioLabs, Beverly, Mass.) were added. After a 1-h incubation at 4°C, the beads were washed twice with 200 μl of binding buffer and subjected to SDS-PAGE. The gp120 was detected using an immunoblotting analysis (see above).

Dye-transfer assay. The COS7 cells were transfected with each Env expression vector (pElucEnv WT, MSD GpA, MSD GpAG831, EnvKO, or MSD VSV-G) by FuGene6 and cocultured with H9 cells at 48 h after transfection. H9 cells used for this assay were loaded with CellTracker CM-DiI (at a final concentration of 10 μM) and Calcein blue, AM (Molecular Probes) (at a final concentration of 40 μM), precultured for 3 h, and then washed with culture medium. At 2 h after coculture, the cells were fixed with 4% paraformaldehyde–PBS and analyzed using a Zeiss LSM510META microscope. Cells showing green, red, or blue fluorescence were counted in each of five randomly selected fields at magnification of ×200.

T7 RNApol transfer assay. The COS7 cells were transfected with each Env expression vector (pElucEnv WT, MSD GpA, MSD GpAG831, MSD VSV-G, or EnvKO) together with pTM3hRL (see above) by the use of FuGene6. At 48 after transfection, the transfected COS7 cells were cocultured with the 293CD4 cells that had been transfected with the T7 RNApol expression vector, pCMMP T7RNApoliresGFP (the ratio of cells was 1:1). At 12 h after coculture, the cells were lysed and the firefly luciferase activities, derived from the Env expression vector, and renilla luciferase activities, activated by the T7 RNApol transferred from 293CD4 cells through the generated fusion pores, were determined using a Dual-Glo luciferase reporter assay system (Promega).

RESULTS

Gly^{sub} mutations did not affect the fusion activity of gp41 in MAGI cells. The amino acid sequences of the predicted MSD of HXB2, the consensus sequences of HIV-1 subtypes, and sequences of certain other membrane proteins are shown in Fig. 1A. Although the MSDs of CD22 and CD4 could replace the MSD of gp41 without affecting its function (41, 45), the lengths of the predicted MSDs differ and there is no apparent sequence homology among them except for the presence of several glycine residues. The amino acid sequence of the MSD of gp41 is well conserved among different clades, and it contains the GXXXG motif. Except for the MSD in CD22, all MSDs listed contain the GXXXG motif. To evaluate the relative contributions that the three glycine residues in the gp41 MSD made to fusion activity, each glycine residue was changed to an alanine or a leucine residue. Additionally, all three glycine residues were changed to alanine residues in the 3A mutant. The amino acid sequences and nomenclatures of Gly^{sub} mutants are shown in Fig. 1B. Alanine and leucine residues were chosen because they are commonly found in the transmembrane region of membrane proteins (39). In a previous study, substituting alanine or leucine residues for glycine residues in VSV-G produced membrane-fusion-incompetent proteins (8).

The protein profile of Gly^{sub} mutants was examined by immunoblotting analysis of both cell and virus lysates derived from COS7 cells transfected with the proviral DNAs. Similar

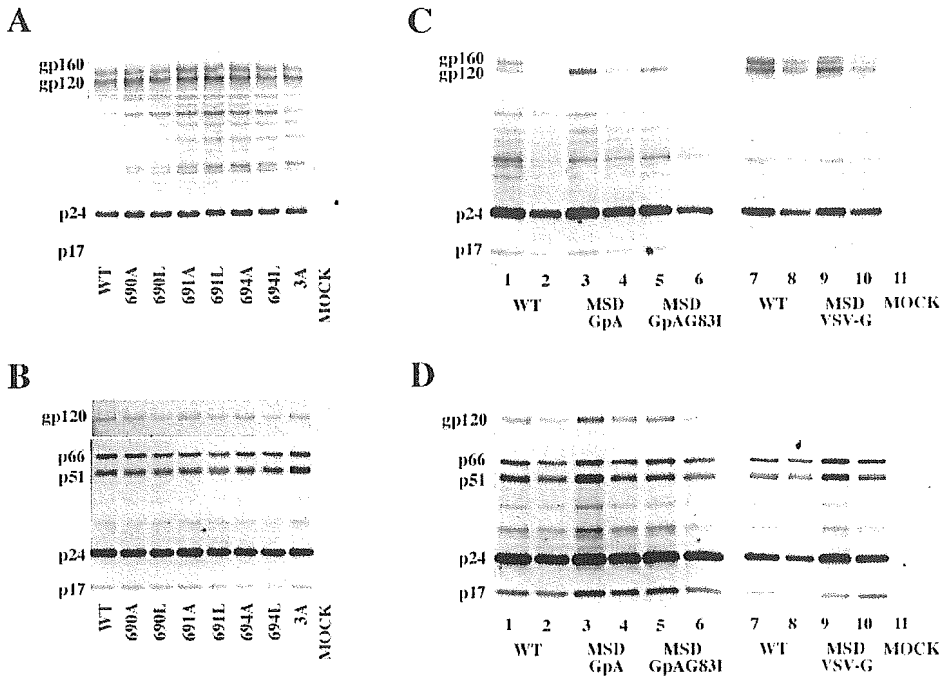

FIG. 2. Protein profiles of cell and virus lysates of the WT and mutants. The cell and virus lysates for glycine substitution (A and B) and MSD replacement mutants (C and D) were prepared from COS7 transfected with proviral DNA. The Env proteins (gp160, gp120) were detected with anti-gp120 polyclonal antibody. Gag (p24, p17) and Pol (p66, p51) were detected using serum from an individual infected with HIV-1. The name of the provirus DNA is indicated below, and the bands corresponding to gp160, gp120, p66, p51, p24, and p17 are shown by arrows. (C and D) For MSD replacement mutants, two different amounts of lysates were loaded for each mutant. The second lane of each sample received an amount of the lysate that was half of the amount used for the preceding lane.

protein profiles were observed for all Gly^{sub} mutants and the WT in both cell and virus lysates (Fig. 2A and B). For all Gly^{sub} mutants, both gp160 and gp120 were detected in cell lysates and gp120 was detected in virus lysates. We did not observe prominent changes in Env processing, as in the case of the MSD replacement (MSD^{rep}) mutants (see below). In virus lysates, similar levels of Env relative to virus Gag/Pol products (p17, p24, p51, and p66) were detected in each sample (Fig. 2B). These data suggested that all the Env mutants were expressed, processed, transported to the plasma membrane, and incorporated onto the virions. Fusion activities of the Gly^{sub} mutants were evaluated by a MAGI cell assay using an arbitrary fusion index that reflects both the number of syncytia and the number of nuclei within a syncytium. As shown in Fig. 3, the fusion index of all Gly^{sub} mutants was comparable with that of the WT. Notably, the fusion activity of the 3A mutant was also well maintained (Fig. 3). These data suggested that glycine residues in the MSD of gp41 were not necessary for membrane fusion in MAGI cells.

Gly^{sub} mutants retained the replication capacity in Jurkat cells. We next evaluated the effect of glycine substitution on viral replication in T-cell lines. Viruses collected from the culture supernatants of COS7 cells transfected with the proviral DNAs were used to infect Jurkat or H9 cells. Replication of mutant viruses was monitored by measuring the amount of p24 released into the culture medium. A representative result is shown in Fig. 4. All Gly^{sub} mutants were replication competent and showed replication kinetics similar to those of the WT virus in Jurkat cells. Similar results were observed in H9 cells (data not shown). These results were consistent with the results of fusion assay in MAGI cells (Fig. 3) and suggested that the contribution of glycine residues in MSD to the life cycle of HIV-1 was relatively small.

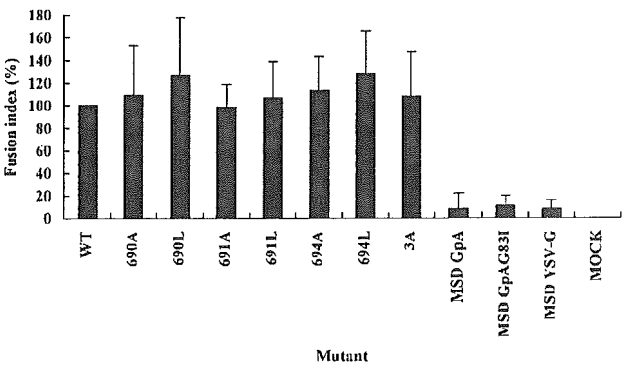

FIG. 3. Relative fusion activity of MSD mutants in MAGI cell assay. Fusion activity of the WT and MSD mutants was expressed using a fusion index (fusion index = $2x + y$, where x is the number of multinucleated cells [number of nuclei ≥ 5 in five visual fields] and y is the number of multinucleated cells [number of nuclei < 5 in five visual fields]). The fusion index was defined to reflect the number of nuclei in multinucleated cells. Fusion activities for each mutant are shown after normalization to that of the WT (the WT activity was set at 100%). Similar results were obtained in three independent experiments.

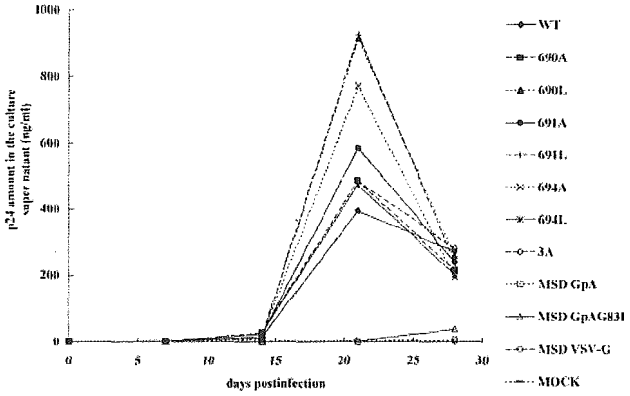

FIG. 4. Replication profiles of the WT and MSD mutants in Jurkat cells. Viral stocks of the WT and each mutant were prepared from culture supernatant of COS7 cells transfected with proviral DNA, and Jurkat cells were infected with each virus adjusted by the amount of p24. Replication was monitored by measuring the amount of p24 in the culture supernatant at specific time points following infection. A representative result of three independent experiments is shown.

The protein profile of MSD^{rep} mutants was altered. Our data for Gly^{sub} mutants suggested that the MSD of gp41 might have a rather high tolerance for mutation. To examine the extent to which the gp41 MSD tolerated more drastic changes in amino acid sequences, the entire MSD of gp41 was replaced with that of VSV-G, GpA, or GpAG83I. The sequence of each MSD is shown in Fig. 1B. Both GpA and VSV-G contain the GXXXG motif within their MSDs. The former takes a dimer, and the latter forms a trimer. The GpAG83I is a GpA mutant that lacks homodimerization activity owing to the substitution of the 83rd glycine residue (the numbering is according to the system used for GpA study) with an isoleucine residue. This GpAG83I was included to overcome the potential negative effect of the homodimerization activity of GpA (34).

The expression of viral gene products from MSD^{rep} mutants was examined by immunoblotting analysis using cell and virus lysates derived from COS7 cells transfected with the proviral DNAs. Two different amounts of each lysate type (cell and virus) were loaded for each construct to achieve semiquantitative evaluation of the band intensity. The second lane of each sample received an amount of the lysate that was half that of the preceding lane. In cell lysates, the reproducible change in the processing pattern of Env was noted for MSD^{rep} mutants. All MSD^{rep} mutants showed more signal for gp120 than for gp160 (Fig. 2C). This was most prominent in GpA and GpAG83I mutants, followed by the VSV-G mutant (Fig. 2C). The sum intensity of gp160/gp120 normalized by the p24 amount was approximately same for both MSD^{rep} mutants and the WT.

This semiquantitative analysis was also performed for virus lysates (Fig. 2D). In virus lysates, the intensity for gp120 relative to p24 was stronger for GpA and GpAG83I mutants (compare lane 1 with lane 4 or 5 in Fig. 2D). Compared with the WT, the VSV-G replacement mutant showed relatively more p24 for an approximately equivalent amount of gp120 (compare lanes 7 and 9 in Fig. 2D). This may indicate that the VSV-G mutant incorporated Env less efficiently than the WT or that Env was shed by the VSV-G mutant. Thus, there were some alterations in expression, processing, and transport to the plasma membrane and in the incorporation onto the virions in Env of MSD^{rep} mutants in the provirus context. Next we evaluated the function of Env of MSD^{rep} mutants.

Fusion activity of MSD^{rep} mutants was significantly decreased. The MAGI cell assay was used to examine the fusion activity of MSD^{rep} mutants. Compared with the WT, far fewer multinucleated cells were observed in MSD^{rep} mutants. Although syncytia were occasionally observed in an MSD^{rep} mutant, each syncytium observed contained fewer nuclei than any given syncytium observed in the WT. Thus, fusion indices of MSD^{rep} mutants were very low compared with those of the WT (Fig. 3). These observations suggested the presence of defects in the membrane fusion steps themselves, because changes in the expression level and the processing of Env in cell lysates (Fig. 2C) alone did not seem to be able to account for the observed severe defect in fusion. These defects were partially compensated for when we used a HeLa–CD4-derived cell line that had a higher level of CD4. In this cell line, the efficiency of syncytia formation and the number of nuclei in a syncytium were increased (data not shown). Consistent with the defect in fusion activity, MSD^{rep} mutants showed severely impaired replication capacity in Jurkat cells (Fig. 4) and in H9 cells (data not shown). We tried to determine the point at which membrane fusion ceased in MSD^{rep} mutants by using the Env expression vector.

The cell surface expression and CD4-binding capacity of Env for MSD^{rep} mutants were similar to those for WT. We constructed the Env expression vectors to analyze the steps of membrane fusion processes of MSD^{rep} mutants (Fig. 5A). First, we examined the cell surface Env expression of MSD^{rep} mutants by transfecting each Env expression vector into COS7 cells and then performing a flow cytometric analysis using an anti-gp120 monoclonal antibody. As the transfected cells expressed GFP derived from the expression vector, cells were gated for GFP first. A representative result is shown in Fig. 5B. The fluorescence intensities of Env in MSD^{rep} mutants and the WT were nearly equal. The expression of Env was also verified by Western blotting analysis (data not shown).

Next, we tested the CD4-binding capacity of the Env of MSD^{rep} mutants, because mutations in MSDs potentially affect the conformation of Env. We immunoprecipitated CD4 by using anti-CD4 antibody from a mixture of cell lysates prepared from COS7 cells that had been transfected with either the CD4 expression vector or the Env expression vector. The gp120 that coimmunoprecipitated with the CD4 was detected using immunoblotting analysis. The gp120 coimmunoprecipitated at similar efficiencies in MSD^{rep} mutants and the WT (Fig. 5C). These data suggested that the MSD replacement did not affect the CD4-binding capacity of the mutated Envs. Thus, the membrane fusion defect of Envs of MSD^{rep} mutants was determined to be in the post-CD4-binding steps.

Examination of the hemifusion and fusion pore formation steps in MSD^{rep} mutants. We used the dye-transfer assay to examine whether Envs of MSD^{rep} mutants were able to induce lipid mixing and fusion pore formation between Env- and receptor-expressing cells. In this assay, the COS7 cells transfected with a recombinant Env expression vector bearing the EGFP-firefly luciferase hybrid gene (Fig. 5A) were cocultured with T cells whose cell membrane and cytoplasm were labeled

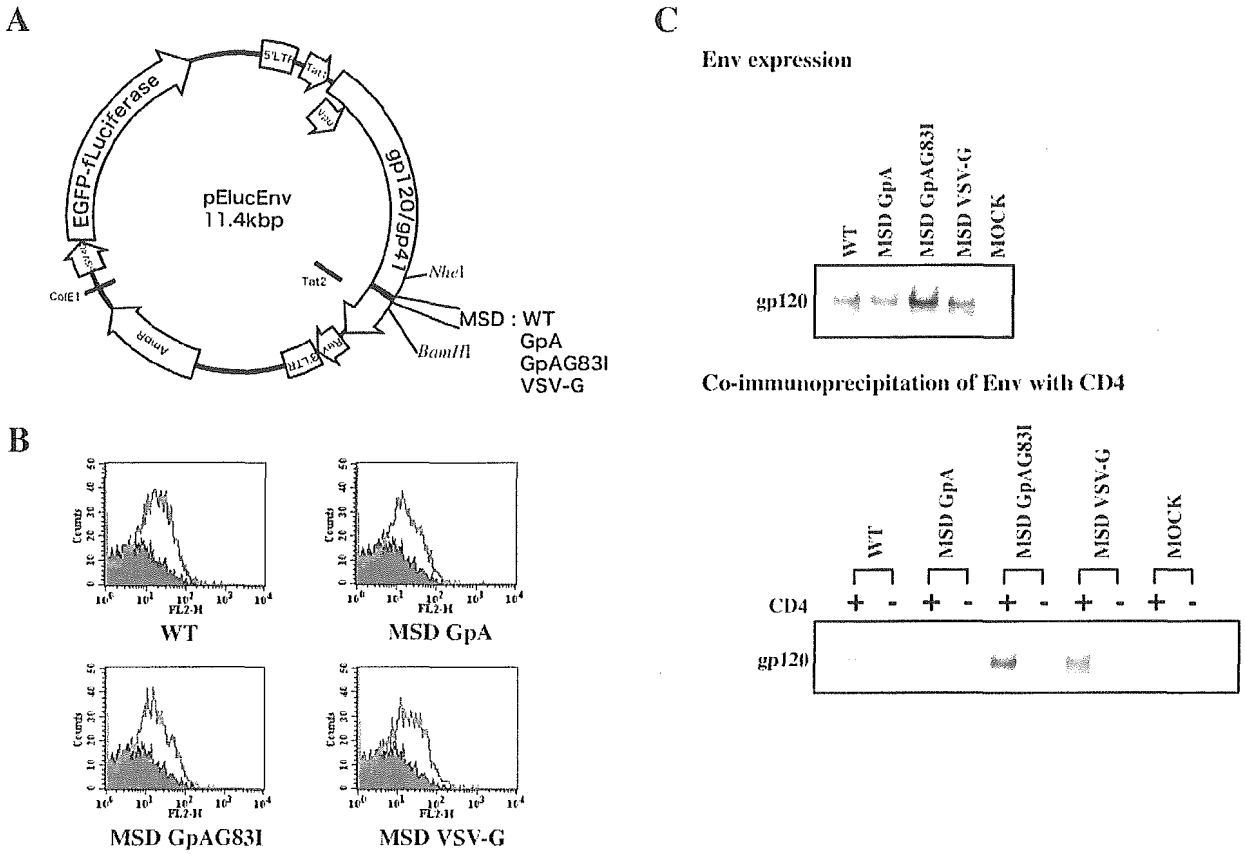

FIG. 5. Evaluation of the cell surface expression and the CD4-binding capacity of Env of MSD mutants. (A) The map of the Env expression vector pElucEnv. pElucEnv supports the expression of HIV-1 *env* (gp120/gp41) and the gene of the EGFP-firefly luciferase (EGFP-fLuciferase) hybrid protein from two separate promoters. The NheI-BamHI fragments of pSP65HXB2RU3ΔN WT, MSD GpA, MSD GpAG83I, or MSD VSV-G were cloned into pElucEnv. 5′LTR, 5′ long terminal repeat of HIV-1; 3′LTR, 3′ long terminal repeat of HIV-1. *tat*, *vpu*, and *rev* represent *tat*, *vpu*, and *rev* of HIV-1. AmpR, beta-lactamase; SV40, simian virus 40 late promoter; ColE1, ColE1 replication origin; NheI and BamHI, restriction sites used for cloning of the mutated *env*. (B) Cell surface expression of Env. COS7 cells were transfected with each pElucEnv construct and subjected to flow cytometric analysis as described in the Materials and Methods section. The signal for each Env is shown with a gray line. The filled area depicts the signal obtained for the control vector, EnvKO. (C) CD4-binding capacity of Env of MSD mutants. The cell lysates prepared from the COS7 cells that had been transfected with the pElucEnv construct or the CD4 expression vector were mixed together, and CD4 was immunoprecipitated using OKT-4. The amount of gp120 coimmunoprecipitated with CD4 was evaluated. The upper panel shows the expression level of each Env mutant. Coimmunoprecipitated gp120 was detected using anti-gp120 polyclonal antibodies (shown in the lower panel).

with CM-DiI (red) and Calcein blue, AM (blue), respectively. When the lipids from the two cells mix, a transfer of red dye should be observed. If fusion pores are formed, fused cells whose cytoplasm bears both blue and green fluorescence should appear. The results are shown in Fig. 6. At 2 h after coculture, cells having green, red, and blue fluorescence were observed in the WT (Fig. 6A). Similar cells were also observed in MSD^{rep} mutants but were fewer in number than those observed in the WT. We determined the frequency of lipid or cytoplasmic mixing 2 h after coculture by counting Env-expressing cells (green cells) whose membrane or cytoplasm was stained with CM-DiI or Calcein blue, AM, respectively. In MSD^{rep} mutants, many Env-expressing COS7 cells were surrounded by T cells and showed no evidence of dye transfer. The relative frequency of dye transfer was determined to be less than half that of the WT (Fig. 6B). In this assay, we did not observe significant discrepancies in the frequencies with which the two dyes were transferred; that is to say, cells arrested at the hemifusion stage were not detected. These data suggested that Env of MSD^{rep} mutants retained the capacity for fusion but at efficiencies that were much lower than those of the WT and that failed to produce large syncytia. The decrease in transfer of CM-DiI indicated that MSD^{rep} mutants had a defect that affected the fusion process prior to hemifusion. The smaller size of the syncytia observed in MSD^{rep} mutants may suggest the presence of other defects after hemifusion, possibly an enlargement of fusion pore.

We performed an additional quantitative assessment of fusion pore formation by the use of the T7 RNApol transfer assay. In this assay, COS7 cells were first transfected with an Env expression vector coupled with a reporter plasmid, pTM3hRL, which encodes T7 promoter-driven renilla luciferase, and then were cocultured with 293CD4 cells that had been transfected with a T7 RNApol expression plasmid. When the COS7 and 293CD4 cells fused, the T7 RNApol in the 293CD4 cells transferred into the COS7 cells and drove ex-

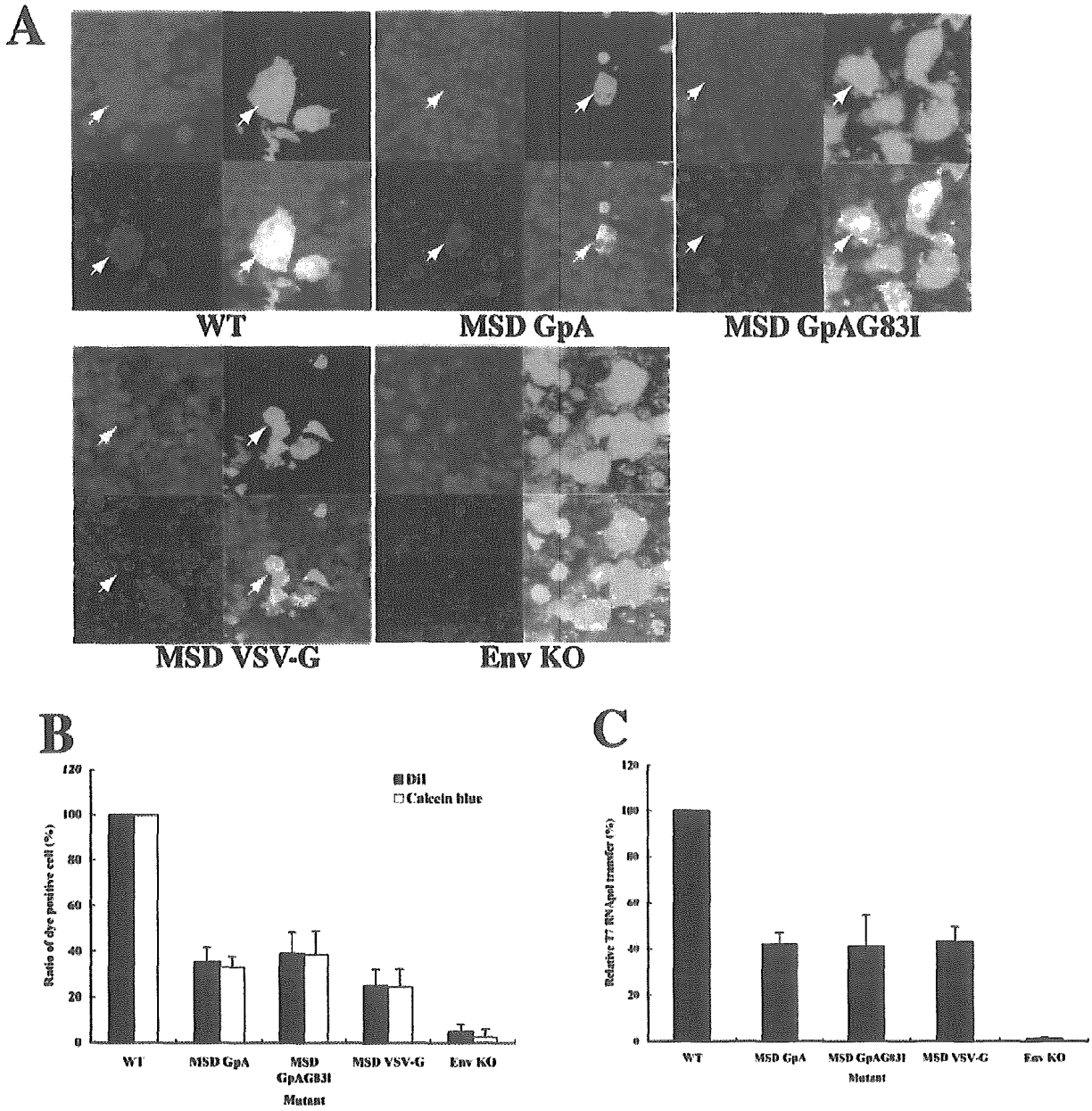

FIG. 6. Cell-cell fusion analysis. The results of a dye-transfer assay using a coculture system and COS and T cells are shown. The COS7 cells transiently transfected with each pElucEnv construct were cocultured with H9 cells that had been loaded with CellTracker CM-DiI (pseudo-red) and Calcein blue, AM (pseudo-blue). Pictures taken at 2 h after coculture are shown in panel A. Typical fused cells having green, red, or blue fluorescence are indicated by arrows. Original magnification, ×200. (B) Relative dye-transfer frequencies of MSD^{rep} mutants. The number of Env-expressing cells (green cells) whose membranes or cytoplasms are labeled with CM-DiI (red) or Calcein blue, AM (blue), respectively, was counted in five, randomly selected fields. The value was established by setting WT at 100%. The averages of the results from four experiments are shown. (C) Results of T7 RNApol-transfer assay to determine fusion pore formation of MSD mutants. The COS7 cells were transfected with each pElucEnv construct and the T7 RNApol-responsive reporter plasmid, pTM3hRL. At 48 h after transfection, the transfected COS7 cells were cocultured with the 293CD4 cells that had been transfected with pCMMP T7RNApoliresGFP. At 12 h after coculture, the cells were lysed and firefly luciferase and renilla luciferase activity levels were measured. Pore formation efficiencies were calculated by comparing the induced renilla luciferase activity to the firefly luciferase activity. A representative result of four independent experiments is shown.

pression of renilla luciferase. At 12 h after coculture, renilla luciferase activities were measured. The value was normalized according to the efficiency of transfection measured by firefly luciferase activities derived from the Env expression vector. Representative results are shown in Fig. 6C. Normalized renilla luciferase activities of MSD GpA, MSD GpAG83I, MSD VSV-G, and EnvKO were, respectively, 42, 41, 43, and 1.3% of that of the WT. Thus, the transfer of T7 RNApol observed for cells that were expressing MSD^{rep} Env was less efficient than that of the WT, a finding consistent with that from the dye-

transfer assay. We also tested a cleavage site mutant of Env (R511S) (3), which cannot produce an active fusion peptide and is unable to induce membrane fusion in this assay. The value was 2.6%. Therefore, the value obtained for MSD^{rep} mutants should reflect the efficiency of de novo pore formation. The value of around 40% of that of the WT obtained for MSD^{rep} mutants may appear high compared with the severe defects in the MAGI assay (Fig. 3) and replication assay (Fig. 4). This could be the result of differences in the two assay systems or it might suggest the presence of additional defects in membrane fusion in MSD^{rep} mutants.

DISCUSSION

The involvement of the MSD in membrane fusion has been studied for several different viruses, including HIV-1 (8, 14, 15, 22, 23, 28, 35, 36, 38, 42). However, the precise molecular mechanism of Env-mediated membrane fusion is not known, and the role of MSD, including whether the specific amino acid sequences in MSD are required for the membrane fusion process, is not well understood. Examination of the presently available HIV-1 sequence database reveals a high conservation of MSD sequences for gp41 (17). There also are several well-conserved glycine residues that form the GXXXG motif, a motif found in the helix-helix interface of many membrane-spanning α-helices (24, 26, 29). Interestingly, the MSDs of CD4 and CD22, which can replace the MSD of gp41 without affecting its fusion activity, also contain several glycine residues. Building from these findings, we investigated whether the specific sequence of the gp41 MSD is required for competent membrane fusion. We did this by mutating the conserved glycine residues in the gp41 MSD to alanine or leucine residues. A similar mutation of glycine introduced into VSV-G has a detrimental effect on membrane fusion (8). Contrary to our expectations, mutation of glycine residues resulted in fusion-competent gp41 (Fig. 3). Even replacing all three glycine residues in gp41 MSD with alanine residues did not affect fusion activity (Fig. 3). This suggests that, in vitro, the gp41 MSD has a rather high tolerance for mutation. The conservation of glycine residues observed in field isolates may indicate that HIV-1 requires glycine residues for in vivo infection of cells whose properties are different from those seen with in vitro T-cell lines. This may also imply that the potential mechanisms involved in membrane fusion differ for gp41 and VSV-G. It may be that the contribution of the proposed kink in the MSD, induced by the presence of a glycine residue during VSV-G-mediated membrane fusion, is not as critical to the membrane fusion process in gp41 as it is for the same process in VSV-G (8). To further verify the role of GXXXG motif for a potential helix-helix association motif, future analyses may require simultaneous substitution of all glycines with other bulky amino acid residues.

Proceeding on the basis of our results obtained with Gly^{sub} mutants and previous reports of replication-competent HIV-1 having heterologous MSD in place of the natural gp41 MSD, we next replaced the entire gp41 MSD with MSDs of heterologous membrane proteins (GpA or VSV-G). Membrane fusion activity was severely impaired in both the GpA and VSV-G replacement mutants (Fig. 3). Because GpA is known to form a dimer through the GXXXG motif, the dimerization activity may interfere with the proper trimerization of gp41 and cause the observed defect. However, the observed defect was not rescued by introducing a G83I mutation within the MSD of GpA (Fig. 3), a mutation that has been shown to knock out the dimerization ability (34). Therefore, the defect cannot be explained simply by noting that replacing the MSD interfered with gp41's proper trimerization. A similar defect in membrane fusion observed in our VSV-G–replacement mutant may further support this argument, because VSV-G, like gp41, is reported to form a trimer. At this time, however, we cannot completely rule out the potential defect in proper trimerization of Env in the MSD replacement mutants.

It is worth mentioning that we observed more gp120 than gp160 reproducibly in MSD^{rep} mutants, especially for GpA-replacement mutants in the transfected cells. This may suggest that there are some subtle conformational changes in Env for the GpA-replacement mutants that allow for more efficient processing by the furin-like protease. It also suggests that the mutation may alter the length of time needed for the mutant envelope proteins to travel through the *trans* Golgi network. These possibilities are consistent with a hypothesis that mutation within the MSD may affect the intracellular trafficking of the envelope protein. We cannot rule out this hypothesis.

In the provirus context, a smaller amount of Env was detected in virus lysates for VSV-G replacement mutant (Fig. 2D). This defect, in addition to the defect in fusion, may contribute to the VSV-G replacement mutant's inability to replicate (Fig. 4). The mechanism of this defect is not known at present. The mutation within the MSD, however, may affect the structure of gp41 and that, in turn, may result in a less efficient interaction between Gag and Env during assembly or a less stable association between gp41 and gp120 in this replacement mutant.

To analyze the effect of the MSD mutation in membrane fusion independent of other viral structural proteins, we used the Env expression vector. We found no significant difference in the steady-state amount of envelope proteins expressed on the cell surface and the CD4-binding efficiency (Fig. 5B). Therefore, the drastic changes in either trafficking or conformation cannot explain the observed prominent defect in fusion activity of GpA or VSV-G replacement mutants. One of the potential defects of membrane fusion in our MSD^{rep} mutants should reside in the post-CD4 binding step(s) of membrane fusion processes. In MSD^{rep} mutants, there may be a difference in the interactions between Env and the chemokine receptors or in the conformational changes induced after such interactions.

The exact defective steps in the membrane fusion mechanism of MSD^{rep} mutants remain to be determined. There should be a defect before the lipid dye mixing step, because we observed decreased efficiency of lipid dye transfer in MSD^{rep} mutants (Fig. 6B). We did not observe the discrepancy between lipid dye (CM-DiI) and cytoplasmic dye (Calecein blue, AM) transfer; therefore, there was no arrest in the hemifusion step. Recently, Lin and coworkers reported that truncating the MSD of simian immunodeficiency virus (SIV) decreased fusion activity (18). As with our mutants, their SIV Env mutants exhibited an overall decrease in lipid dye transfer as well as in cytoplasmic dye transfer. Theirs, however, showed a further downstream defect, namely, an enlargement of the fusion pore

induced by mutated Env. This was suggested by the difference in the efficiency of transfer between low-molecular-weight molecules (Calcein blue, AM) and larger molecules (enhanced blue fluorescent protein). We did not observe this difference in our assay. They also observed the gap between the lipid dye transfer and luciferase transfer assays. In our mutants, the decrease in the lipid dye transfer correlated well with the decrease in the transfer of T7 RNApol assay (Fig. 6B and C). The discrepancy between the studies might arise from the differences between the two viruses (SIV and HIV) or from the nature of the mutations introduced (truncation versus replacement).

We observed a pore formation efficiency of approximately 40% for the MSD^{rep} mutants compared with that observed with the WT despite their prominent fusion defect observed in MAGI cells. Because the two assays described in Fig. 3 and 6 employed different cell types and expression systems, it may be difficult to compare these two assays directly. There is the possibility that the discrepancy between the assays was artificially enhanced by the differences in the two assay systems. For example, the levels of expressed Env and of CD4 were higher in the T7 RNApol transfer assay than in the MAGI cell assay (data not shown). When a higher CD4-expressing cell line was used in the fusion assay instead of the MAGI cells, while maintaining with the provirus constructs, the efficiency of fusion was increased (data not shown). When the provirus constructs were used instead of the Env expression vectors in the T7 RNApol transfer assay, the values for pore formation were slightly decreased. The individual values of GpA, GpAG83I, and VSV-G were 39, 27, and 20%, respectively. The value for the mock treatment was about 1%. Thus, the observed gap could be accounted for in part by the difference in assay systems. However, very inefficient formation of the large syncytia in MSD^{rep} mutants might indeed suggest the presence of the defect in the steps after the formation of initial fusion pores.

Our data on MSD^{rep} mutants clearly demonstrate that not all heterologous MSDs can replace the gp41 MSD without affecting its function. The data indicate that the expression or retention of gp41 on the lipid bilayer and the fusion activity itself are rather independent functions. Our results also show that the mere maintenance of the GXXXG motif is not sufficient for fusion activity. It seems likely that a context-dependent arrangement of the glycine and other amino acid residues within the MSD is critical for functional integrity.

In this study, we have provided evidence that the MSD of gp41 affects the biogenesis of Env and also plays a critical role in membrane fusion for HIV-1. As our results for the Gly^{sub} and MSD^{rep} mutants suggest, the gp41 MSD shows a rather high tolerance for mutation but does require the MSD to have some specific sequences—or structures generated by them—for its proper function. One possible scenario is that the gp41 MSD may interact with some lipid or protein components during membrane fusion. Such an interaction between Env and lipid or protein moieties has been reported for the Semliki Forest virus and the influenza virus, respectively (2, 19). The gp41 MSDs might interact among themselves, with fusion peptides, or with the MSDs of other host proteins, such as CD4 or chemokine receptors, that are thought to come within close proximity of one another during the membrane fusion process. A failure to properly interact because of mutations in the gp41 MSD may affect the fusion process. To address these issues, additional systematic mutagenesis studies are needed to determine the critical residues of the MSD. Such studies should shed light on the molecular mechanisms of membrane fusion. Elucidating the precise molecular mechanism of membrane fusion—and the role of the gp41 MSD in it—may provide another target for a molecular intervention in HIV-1 infection.

ACKNOWLEDGMENTS

This study was supported by the Health and Labour Sciences Research Grants from Japanese Ministry of Health, Labor, and Welfare.

We thank A. M. Menting for assistance in manuscript preparation.

REFERENCES

1. **Aoki, Y., H. Aizaki, T. Shimoike, H. Tani, K. Ishii, I. Saito, Y. Matsuura, and T. Miyamura.** 1998. A human liver cell line exhibits efficient translation of HCV RNAs produced by a recombinant adenovirus expressing T7 RNA polymerase. Virology **250**:140–150.
2. **Armstrong, R. T., A. S. Kushnir, and J. M. White.** 2000. The transmembrane domain of influenza hemagglutinin exhibits a stringent length requirement to support the hemifusion to fusion transition. J. Cell Biol. **151**:425–437.
3. **Bosch, V., and M. Pawlita.** 1990. Mutational analysis of the human immunodeficiency virus type 1 *env* gene product proteolytic cleavage site. J. Virol. **64**:2337–2344.
4. **Bullough, P. A., F. M. Hughson, J. J. Skehel, and D. C. Wiley.** 1994. Structure of influenza haemagglutinin at the pH of membrane fusion. Nature **371**:37–43.
5. **Chan, D. C., D. Fass, J. M. Berger, and P. S. Kim.** 1997. Core structure of gp41 from the HIV envelope glycoprotein. Cell **89**:263–273.
6. **Chen, J., S. A. Wharton, W. Weissenhorn, L. J. Calder, F. M. Hughson, J. J. Skehel, and D. C. Wiley.** 1995. A soluble domain of the membrane-anchoring chain of influenza virus hemagglutinin (HA2) folds in *Escherichia coli* into the low-pH-induced conformation. Proc. Natl. Acad. Sci. USA **92**:12205–12209.
7. **Chesebro, B., and K. Wehrly.** 1988. Development of a sensitive quantitative focal assay for human immunodeficiency virus infectivity. J. Virol. **62**:3779–3788.
8. **Cleverley, D. Z., and J. Lenard.** 1998. The transmembrane domain in viral fusion: essential role for a conserved glycine residue in vesicular stomatitis virus G protein. Proc. Natl. Acad. Sci. USA **95**:3425–3430.
9. **Dubay, J. W., S. J. Roberts, B. H. Hahn, and E. Hunter.** 1992. Truncation of the human immunodeficiency virus type 1 transmembrane glycoprotein cytoplasmic domain blocks virus infectivity. J. Virol. **66**:6616–6625.
10. **Eisenberg, D., and M. Wesson.** 1990. The most highly amphiphilic alpha-helices include two amino acid segments in human immunodeficiency virus glycoprotein 41. Biopolymers **29**:171–177.
11. **Fass, D., S. C. Harrison, and P. S. Kim.** 1996. Retrovirus envelope domain at 1.7 angstrom resolution. Nat. Struct. Biol. **3**:465–469.
12. **Fleming, K. G., and D. M. Engelman.** 2001. Specificity in transmembrane helix-helix interactions can define a hierarchy of stability for sequence variants. Proc. Natl. Acad. Sci. USA **98**:14340–14344.
13. **Freed, E. O., and M. A. Martin.** 1996. Domains of the human immunodeficiency virus type 1 matrix and gp41 cytoplasmic tail required for envelope incorporation into virions. J. Virol. **70**:341–351.
14. **Harman, A., H. Browne, and T. Minson.** 2002. The transmembrane domain and cytoplasmic tail of herpes simplex virus type 1 glycoprotein H play a role in membrane fusion. J. Virol. **76**:10708–10716.
15. **Kemble, G. W., T. Danieli, and J. M. White.** 1994. Lipid-anchored influenza hemagglutinin promotes hemifusion, not complete fusion. Cell **76**:383–391.
16. **Kimpton, J., and M. Emerman.** 1992. Detection of replication-competent and pseudotyped human immunodeficiency virus with a sensitive cell line on the basis of activation of an integrated β-galactosidase gene. J. Virol. **66**:2232–2239.
17. **Kuiken, C., B. Foley, B. Hahn, P. Marx, F. McCutchan, J. Mellors, S. Wolinsky, and B. Korber.** 2001. *HIV Sequence Compendium* 2001. Theoretical Biology and Biophysics Group, Los Alamos National Laboratory, Los Alamos, N.M.
18. **Lin, X., C. A. Derdeyn, R. Blumenthal, J. West, and E. Hunter.** 2003. Progressive truncations C terminal to the membrane-spanning domain of simian immunodeficiency virus Env reduce fusogenicity and increase concentration dependence of Env for fusion. J. Virol. **77**:7067–7077.
19. **Lu, Y. E., T. Cassese, and M. Kielian.** 1999. The cholesterol requirement for Sindbis virus entry and exit and characterization of a spike protein region involved in cholesterol dependence. J. Virol. **73**:4272–4278.
20. **Malashkevich, V. N., B. J. Schneider, M. L. McNally, M. A. Milhollen, J. X. Pang, and P. S. Kim.** 1999. Core structure of the envelope glycoprotein GP2 from Ebola virus at 1.9-A resolution. Proc. Natl. Acad. Sci. USA **96**:2662–2667.

21. **Matsuda, Z., X. Yu, Q. C. Yu, T. H. Lee, and M. Essex.** 1993. A virion-specific inhibitory molecule with therapeutic potential for human immunodeficiency virus type 1. Proc. Natl. Acad. Sci. USA **90**:3544–3548.
22. **Melikyan, G. B., S. Lin, M. G. Roth, and F. S. Cohen.** 1999. Amino acid sequence requirements of the transmembrane and cytoplasmic domains of influenza virus hemagglutinin for viable membrane fusion. Mol. Biol. Cell. **10**:1821–1836.
23. **Melikyan, G. B., R. M. Markosyan, M. G. Roth, and F. S. Cohen.** 2000. A point mutation in the transmembrane domain of the hemagglutinin of influenza virus stabilizes a hemifusion intermediate that can transit to fusion. Mol. Biol. Cell **11**:3765–3775.
24. **Mendrola, J. M., M. B. Berger, M. C. King, and M. A. Lemmon.** 2002. The single transmembrane domains of ErbB receptors self-associate in cell membranes. J. Biol. Chem. **277**:4704–4712.
25. **Miller, M. A., R. F. Garry, J. M. Jaynes, and R. C. Montelaro.** 1991. A structural correlation between lentivirus transmembrane proteins and natural cytolytic peptides. AIDS Res. Hum. Retrovir. **7**:511–519.
26. **Mingarro, I., P. Whitley, M. A. Lemmon, and G. von Heijne.** 1996. Ala-insertion scanning mutagenesis of the glycophorin A transmembrane helix: a rapid way to map helix-helix interactions in integral membrane proteins. Protein Sci. **5**:1339–1341.
27. **Murakami, T., S. Ablan, E. O. Freed, and Y. Tanaka.** 2004. Regulation of human immunodeficiency virus type 1 Env-mediated membrane fusion by viral protease activity. J. Virol. **78**:1026–1031.
28. **Odell, D., E. Wanas, J. Yan, and H. P. Ghosh.** 1997. Influence of membrane anchoring and cytoplasmic domains on the fusogenic activity of vesicular stomatitis virus glycoprotein G. J. Virol. **71**:7996–8000.
29. **Op De Beeck, A., R. Montserret, S. Duvet, L. Cocquerel, R. Cacan, B. Barberot, M. Le Maire, F. Penin, and J. Dubuisson.** 2000. The transmembrane domains of hepatitis C virus envelope glycoproteins E1 and E2 play a major role in heterodimerization. J. Biol. Chem. **275**:31428–31437.
30. **Ory, D. S., B. A. Neugeboren, and R. C. Mulligan.** 1996. A stable human-derived packaging cell line for production of high titer retrovirus/vesicular stomatitis virus G pseudotypes. Proc. Natl. Acad. Sci. USA **93**:11400–11406.
31. **Owens, R. J., C. Burke, and J. K. Rose.** 1994. Mutations in the membrane-spanning domain of the human immunodeficiency virus envelope glycoprotein that affect fusion activity. J. Virol. **68**:570–574.
32. **Piller, S. C., J. W. Dubay, C. A. Derdeyn, and E. Hunter.** 2000. Mutational analysis of conserved domains within the cytoplasmic tail of gp41 from human immunodeficiency virus type 1: effects on glycoprotein incorporation and infectivity. J. Virol. **74**:11717–11723.
33. **Pincus, S. H., K. Wehrly, and B. Chesebro.** 1989. Treatment of HIV tissue culture infection with monoclonal antibody-ricin A chain conjugates. J. Immunol. **142**:3070–3075.
34. **Russ, W. P., and D. M. Engelman.** 2000. The GxxxG motif: a framework for transmembrane helix-helix association. J. Mol. Biol. **296**:911–919.
35. **Salzwedel, K., P. B. Johnston, S. J. Roberts, J. W. Dubay, and E. Hunter.** 1993. Expression and characterization of glycophospholipid-anchored human immunodeficiency virus type 1 envelope glycoproteins. J. Virol. **67**: 5279–5288.
36. **Shmulevitz, M., J. Salsman, and R. Duncan.** 2003. Palmitoylation, membrane-proximal basic residues, and transmembrane glycine residues in the reovirus p10 protein are essential for syncytium formation. J. Virol. **77**:9769–9779.
37. **Tan, K., J. Liu, J. Wang, S. Shen, and M. Lu.** 1997. Atomic structure of a thermostable subdomain of HIV-1 gp41. Proc. Natl. Acad. Sci. USA **94**: 12303–12308.
38. **Taylor, G. M., and D. A. Sanders.** 1999. The role of the membrane-spanning domain sequence in glycoprotein-mediated membrane fusion. Mol. Biol. Cell **10**:2803–2815.
39. **Ulmschneider, M. B., and M. S. Sansom.** 2001. Amino acid distributions in integral membrane protein structures. Biochim. Biophys. Acta **1512**:1–14.
40. **Venable, R. M., R. W. Pastor, B. R. Brooks, and F. W. Carson.** 1989. Theoretically determined three-dimensional structures for amphipathic segments of the HIV-1 gp41 envelope protein. AIDS Res. Hum. Retrovir. **5**:7–22.
41. **Vincent, M. J., N. U. Raja, and M. A. Jabbar.** 1993. Human immunodeficiency virus type 1 Vpu protein induces degradation of chimeric envelope glycoproteins bearing the cytoplasmic and anchor domains of CD4: role of the cytoplasmic domain in Vpu-induced degradation in the endoplasmic reticulum. J. Virol. **67**:5538–5549.
42. **Weiss, C. D., and J. M. White.** 1993. Characterization of stable Chinese hamster ovary cells expressing wild-type, secreted, and glycosylphosphatidylinositol-anchored human immunodeficiency virus type 1 envelope glycoprotein. J. Virol. **67**:7060–7066.
43. **Weissenhorn, W., A. Carfi, K. H. Lee, J. J. Skehel, and D. C. Wiley.** 1998. Crystal structure of the Ebola virus membrane fusion subunit, GP2, from the envelope glycoprotein ectodomain. Mol. Cell **2**:605–616.
44. **Weissenhorn, W., A. Dessen, S. C. Harrison, J. J. Skehel, and D. C. Wiley.** 1997. Atomic structure of the ectodomain from HIV-1 gp41. Nature **387**: 426–430.
45. **Wilk, T., T. Pfeiffer, A. Bukovsky, G. Moldenhauer, and V. Bosch.** 1996. Glycoprotein incorporation and HIV-1 infectivity despite exchange of the gp160 membrane-spanning domain. Virology **218**:269–274.
46. **Yu, X., X. Yuan, M. F. McLane, T. H. Lee, and M. Essex.** 1993. Mutations in the cytoplasmic domain of human immunodeficiency virus type 1 transmembrane protein impair the incorporation of Env proteins into mature virions. J. Virol. **67**:213–221.

Available online at www.sciencedirect.com
SCIENCE DIRECT
Experimental Cell Research 308 (2005) 29–40
Experimental Cell Research
www.elsevier.com/locate/yexcr

Distinct IκB kinase regulation in adult T cell leukemia and HTLV-I-transformed cells

Hideyasu Miura[a], Michiyuki Maeda[b], Naoki Yamamoto[a,c], Shoji Yamaoka[a,*]

[a]*Department of Molecular Virology, Graduate School of Medicine, Tokyo Medical and Dental University, 1-5-45 Bunkyo-ku, Tokyo 113-8519, Japan*
[b]*Laboratory of Infection and Prevention, Department of Biological Responses, Institute for Virus Research, Kyoto University, Kyoto, Japan*
[c]*AIDS Research Center, National Institute of Infectious Diseases, Tokyo, Japan*

Received 7 October 2004, revised version received 6 April 2005
Available online 4 May 2005

Abstract

We have recently shown constitutive IκB kinase (IKK) activation and aberrant p52 expression in adult T cell leukemia (ATL) cells that do not express human T cell leukemia virus type I (HTLV-I) Tax, but the mechanism of IKK activation in these cells has remained unknown. Here, we demonstrate distinct regulation of IKK activity in ATL and HTLV-I-transformed T cells in response to protein synthesis inhibition or arsenite treatment. Protein synthesis inhibition for 4 h by cycloheximide (CHX) barely affects IKK activity in Tax-positive HTLV-I-transformed cells, while it diminishes IKK activity in Tax-negative ATL cells. Treatment of ATL cells with a proteasome inhibitor MG132 prior to protein synthesis inhibition reverses the inhibitory effect of CHX, and MG132 alone greatly enhances IKK activity. In addition, treatment of HTLV-I-transformed cells with arsenite for 1 h results in down-regulation of IKK activity without affecting Tax expression, while 8 h of arsenite treatment does not impair IKK activity in ATL cells. These results indicate that a labile protein sensitive to proteasome-dependent degradation governs IKK activation in ATL cells, and suggest a molecular mechanism of IKK activation in ATL cells distinct from that in HTLV-I-transformed T cells.

Keywords: ATL; HTLV-I; IKK; Proteasome; Arsenite

Introduction

Adult T cell leukemia (ATL) is an aggressive malignancy of CD4+ T lymphocytes that is etiologically associated with human T cell leukemia virus type I (HTLV-I) [1–4]. The cumulative risk of ATL among HTLV-I carriers has been estimated at 1–5%, and those who develop the disease usually have a 40- to 70-year latency period after the time of infection [5]. Cellular transcription factors nuclear factor-κB (NF-κB) [6] and AP-1 [7] are constitutively activated in ATL cells, although the mechanisms of activation remain unknown.

NF-κB is a family of transcription factors that regulates expression of a variety of genes involved in immunological responses, cell growth, angiogenesis, cell-adhesion, and apoptosis [8,9]. Deregulation of NF-κB activity has been increasingly implicated in neoplastic transformation and cancer progression [10–12]. The NF-κB family of transcription factors includes RelA, RelB, c-Rel, NF-κB1 p50, and NF-κB2 p52 [8,13]. In resting cells, the majority of NF-κB is localized in the cytoplasm where it is tightly bound to the inhibitory proteins called inhibitor of NF-κB (IκB). In most cases, activation of NF-κB is preceded by phosphorylation of IκBs by IκB kinase (IKK) complex and subsequent proteasome-dependent degradation of the inhibitors, which results in the release of active NF-κB components to the nucleus. The core of the IKK complex is comprised of two catalytic subunits, IKK1/α and IKK2/β [14–17], and a scaffold protein NF-κB Essential Modulator (NEMO)/IKKγ [18,19]. Recent studies have revealed two distinct pathways of NF-κB activation. The

* Corresponding author. Fax: +81 3 5803 0124.
E-mail address: shojmmb@tmd.ac.jp (S. Yamaoka).

0014-4827/$ - see front matter © 2005 Elsevier Inc. All rights reserved.
doi:10.1016/j.yexcr.2005.04.005

canonical pathway is triggered by many inflammatory stimuli including tumor necrosis factor α (TNF-α) and interleukin 1 (IL-1), depends on IKK2 and NEMO, and induces specific phosphorylation of IκB proteins. Canonical IKK activation initially results in nuclear translocation of p50/RelA heterodimers, which then up-regulate transcription of other NF-κB components. The non-canonical pathway is triggered by a limited number of stimuli including lymphotoxin-β (LT-β) [20–23], B cell activating factor (BAFF) belonging to the TNF family [24,25], TNF-like weak inducer of apoptosis (TWEAK) [26], and CD40 ligand (CD40L) [27] that function in the development, organization, and proper function of tissues. This pathway involves the phosphorylation-dependent processing of NF-κB2 p100 to p52, which requires functional IKK1 and NIK, resulting in nuclear translocation of RelB-containing dimers. In sharp contrast to the canonical NF-κB activation, in which protein synthesis inhibition does not affect IKK activation or nuclear translocation of NF-κB upon ligand binding, the processing of p100 is sensitive to prior treatment of cells with a protein synthesis inhibitor cycloheximide (CHX) [23,24,26,27].

Previous studies on HTLV-I Tax uncovered a unique mechanism by which this viral protein persistently activates NF-κB. Tax activates the IKK complex in a NEMO-dependent manner [18], and in the meantime recruits p100 through its physical interaction with p100, leading to the phosphorylation and processing of p100 [28]. While Tax is readily detected in T cell lines established in vitro by HTLV-I infection and is believed to play important roles in the course of HTLV-I-induced leukemogenesis, its expression is often under detectable level in fresh ATL cells and ATL-derived cell lines. We recently reported constitutive IKK activity and aberrant expression of p52 in ATL cells that do not express detectable Tax protein [29]. These findings suggest that the Tax-independent constitutive NF-κB activation in ATL cells involves engagement of the non-canonical signaling pathway. We show in this report a marked contrast with the response of ATL and HTLV-I-transformed cells to protein synthesis or IKK inhibitors, which further supports the notion that IKK activation in ATL cells is mechanistically different from that by Tax and virtually mediated by the non-canonical NF-κB signaling.

Materials and methods

Cells

ED40515(−) [30], MT-1 [31], and TL-OmI [32] are HTLV-I-infected cell lines of leukemic cell origin. HUT-102 is an HTLV-I-infected non-leukemic cell line established from a patient with cutaneous T cell lymphoma [33]. MT-2 [34] and SLB-1 [35] are human T cell lines transformed in vitro by co-culture with ATL patient-derived leukemic cells. These T cell lines were maintained in RPMI1640 medium supplemented with 10% fetal bovine serum, 100 U/ml penicillin G, and 100 μg/ml streptomycin sulfate.

Reagents

Cycloheximide was purchased from Wako Pure Chemical Industries (Osaka, Japan). MG132 was obtained from Peptide Institute (Osaka, Japan). Sodium arsenite was purchased from Sigma (MO). GST-IκBα (1–72) was purified from *E. coli* transformed with pGEX-KT IκBα (1–72) [18].

Antibodies

Anti-Tax monoclonal antibody (MI73) [36] and anti-NEMO serum [18] were described previously. Anti-α-tubulin monoclonal antibody (DM1A) was purchased from Sigma. Anti-IKK1 monoclonal antibody (B78-1) was obtained from Becton Dickinson Pharmingen (CA). Anti-IκBα antibody (C-21), anti-IKK1 polyclonal antibody (H-744) and anti-IKK2 polyclonal antibody (H-470) were purchased from Santa Cruz Biotechnology (CA).

Preparation of cell extracts

Cells were lysed in Buffer A [20 mM HEPES, pH 7.8, 0.15 mM EDTA, 0.15 mM EGTA, 10 mM KCl, 0.5 mM phenylmethylsulfonyl fluoride (PMSF), 1 μg/ml leupeptin, 1 μg/ml pepstatin A and 1% Nonidet P-40 (NP-40)] supplemented with 100 μM sodium vanadate, and 20 mM β-glycerol phosphate. After centrifugation at 14,000 rpm for 5 min, supernatants were used as cytoplasmic extracts. For preparation of whole cell extract, cells were lysed in RIPA buffer (10 mM Tris/HCl, pH 7.4, 1 mM EDTA, 150 mM NaCl, 1% NP-40, 0.1% sodium deoxycholate, 0.1% SDS, supplemented with 0.5 mM PMSF, 1 μg/ml leupeptin, and 1 μg/ml pepstatin A). Protein concentrations were determined with BCA Protein Assay Kit (Pierce, Erembodegem, Belgium).

Kinase assay

Kinase assay was performed in parallel with immunoblotting following immunoprecipitation with NEMO antiserum. Immunoprecipitation was performed as described previously [37]. Kinase reactions were carried out at 30°C for 30 min in reaction mixture [20 mM HEPES, pH 7.5, 10 mM $MgCl_2$, 50 mM NaCl, 100 μM sodium vanadate, 20 mM β-glycerol phosphate, 2 mM dithiothreitol, 20 μM ATP, 5 μCi [γ-^{32}P]ATP and 1 μg of GST-IκBα (1–72)]. Reactions were fractionated on a 12% SDS-polyacrylamide gel, and phosphorylated GST-IκBα (1–72) was detected by autoradiography. The intensity of each band was determined by computerized image analysis.

Immunoblotting

Proteins in whole cell extracts were fractionated on 8 or 9% SDS-polyacrylamide gels, transferred onto Immobilon membranes, and blots were revealed with an enhanced chemiluminescence detection system (Perkin Elmer Life Science Inc., MA). When necessary, membranes were incubated in stripping buffer (62.5 mM Tris/HCl, pH 6.8, 100 mM 2-mercaptoethanol, 2% SDS) for 30 min at 50°C with constant agitation, washed, and reprobed with another antibody. The intensity of each band was determined by computerized image analysis.

Electorophoretic mobility shift assay (EMSA)

Nuclear extracts were prepared as described previously [37] and incubated with 0.5 ng of ^{32}P-labeled κB probe (KBF1) [38] in binding buffer [10 mM HEPES, pH 7.8, 100 mM NaCl, 1 mM EDTA, 2.5% glycerol, 0.5 μg of poly(dI–dC)] for 30 min at room temperature. Samples were fractionated on a 5% polyacrylamide gel in 0.5% TBE and visualized by autoradiography.

Results

IKK activity in ATL cells is sensitive to protein synthesis inhibition

While the processing of p100 induced by CD40 [27], LT-β [23], or TWEAK [26] was shown to be sensitive to protein synthesis inhibition, little is known about the regulation of IKK or p52 generation in tumor cells with constitutive NF-κB activity. We have recently demonstrated constitutive IKK activity and aberrant p52 expression in Tax-negative ATL cell lines of leukemic cell origin [29]. We previously demonstrated that constitutive IKK activity leading to the processing of p100 was diminished by protein synthesis inhibition in a rat fibroblast cell line [37]. These results prompted us to investigate how protein synthesis inhibition affects IKK activity in a panel of HTLV-I-infected T cell lines. In general, IKK activity in Tax-positive HTLV-I-transformed cells was higher than in Tax-negative cells, probably because of the potency of Tax in IKK activation. Treatment with CHX for 4 h induced marked reduction of IKK activity in Tax-negative ATL cells [ED40515(−), MT-1, and TL-OmI], which contrasted to the sustained IKK activity in Tax-positive HTLV-I-transformed cells (HUT-102, MT-2, and SLB-1) (Figs. 1A and B). Immunoblotting studies revealed that the CHX treatment did not significantly alter steady-state levels of the components of the IKK complex (Fig. 1C). The CHX treatment reduced Tax expression a little, but did not profoundly impair IKK activity in HTLV-I-transformed cells (Fig. 1). We previously described phosphorylation of IκBα in ATL cells [29]. The steady-state levels of IκBα in ATL cells were slightly reduced, but not profoundly affected following protein synthesis inhibition, whereas this protein in HTLV-I-transformed cells, although its steady-state levels are lower than in ATL cells, virtually disappeared (Figs. 1C and D). This different kinetics of IκBα verifies that the in vitro kinase assay results reflect the actual IKK activity in vivo.

Proteasome regulates IKK activity in ATL cells

We next asked if the effect of CHX on IKK activity in ATL cells is due to proteasome-dependent turnover of proteins. Cells were pretreated with a proteasome inhibitor MG132 for 30 min and then exposed to CHX for 4 h in the presence of MG132. As shown in Fig. 2, IKK activity diminished by CHX treatment alone in ATL cells was significantly restored by the combined use of MG132 and CHX. Notably, treatment with MG132 alone greatly enhanced IKK activity in ATL cells. This kinase activation did not alter the steady-state levels of IκBα in ATL cells (Fig. 1D), probably because MG132 blocked phosphorylation-dependent proteasomal degradation of this protein. Treatment of HTLV-I-transformed cells with MG132 remarkably elevated steady-state levels of IκBα, suggesting a very rapid proteasome-dependent turnover of IκBα in Tax-expressing cells (Fig. 1D). MG132 did not affect expression of Tax or components of the IKK complex (Fig. 1C). When cells were treated reciprocally with CHX for 1 h and then incubated with MG132 for 3 h in the presence of CHX (Figs. 3A and B), MG132 failed to restore IKK activity. These results suggest that IKK activation in ATL cells requires continued synthesis of a labile protein that is sensitive to proteasome-dependent degradation. Treatment of Tax-positive HTLV-I-transformed cells with MG132 did not affect IKK activity (Figs. 3C and D).

Distinct responses of ATL and HTLV-I-transformed cells to arsenite

Previous studies revealed that arsenite inhibited IKK activation by binding to Cys-179 in the activation loop of the IKK catalytic subunits [39]. We have examined how arsenite acts on IKK activity in a panel of HTLV-I-infected cells. Arsenite treatment resulted in marked decrease in IKK activity in all the HTLV-I-transformed cells tested (Figs. 4A and B). In sharp contrast to Tax-positive HTLV-I-transformed cells, IKK activity in ATL cells was rather elevated after 8 h of arsenite treatment (Figs. 4F and G). Although immunoblotting studies revealed that the levels of IKK1 and IKK2 in MT-2 and SLB1 cells, but not in HUT-102 cells, appeared to decline in the presence of arsenite (Fig. 4C), we found equivalent amounts of IKK1 in the kinase assay reactions (Fig. 4A, lower panel). We also noted a dose-dependent increase in the amount of IκBα in HTLV-I-transformed cells treated with arsenite (Figs. 4C and D). Consequently, NF-κB DNA binding activity in HTLV-I-

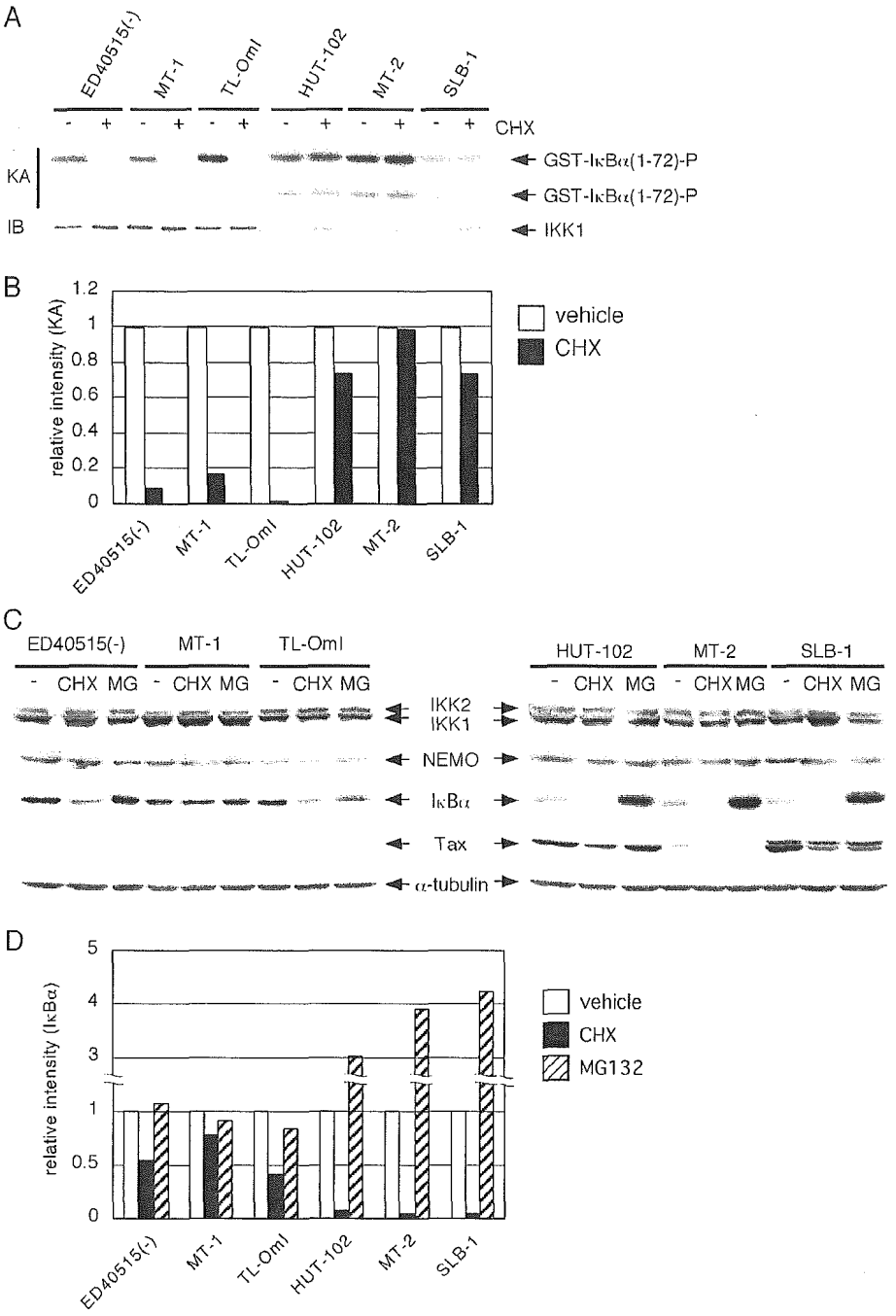

Fig. 1. Protein synthesis inhibition ablates IKK activity in ATL cells. (A) Cells were treated with vehicle (H_2O) or CHX (50 μg/ml) for 4 h. Cytoplasmic extracts (600 μg) were subjected to immunoprecipitation with NEMO antiserum, and immunoprecipitates were used for in vitro kinase assay (KA, upper and middle panels) and detection of IKK1 by immunoblotting (IB, lower panel). Right upper and middle panels show longer and shorter exposures of the same gel, respectively. (B) Relative band intensity of phosphorylated GST-IκBα (1–72) was normalized to the corresponding immunoprecipitated IKK1 band intensity. A value of 1.0 represents normalized phosphorylated GST-IκBα (1–72) band intensity obtained in each control experiment: open bar, vehicle control; closed bar, 50 μg/ml cycloheximide. (C) Cells were treated with RPMI, CHX (50 μg/ml), or MG132 (MG; 20 μM) for 4 h. Whole cell extracts (50 μg) were resolved by SDS-polyacrylamide gel electrophoresis and subjected to immunoblotting for detection of IKK1, IKK2, NEMO, IκBα, Tax, and α-tubulin. (D) Relative band intensity of IκBα was normalized to the corresponding α-tubulin band intensity. A value of 1.0 represents normalized IκBα band intensity obtained in each control experiment: open bar, vehicle control; closed bar, 50 μg/ml cycloheximide; scratched bar, 20 μM MG132. The experiments were carried out at least three times and the results were essentially reproducible.

transformed cells decreased following treatment with arsenite for 12 h (Fig. 4E). On the contrary, dose-dependent decrease in the amount of IκBα was evident in ATL cells (Figs. 4H and I). As expected, EMSA showed increased NF-κB DNA binding activity in ATL cells treated with arsenite for 12 h (Fig. 4J). These responses of IκBα and NF-κB DNA binding activity indicate that the in vitro kinase assay results reflect the actual IKK activity in vivo. Consistent

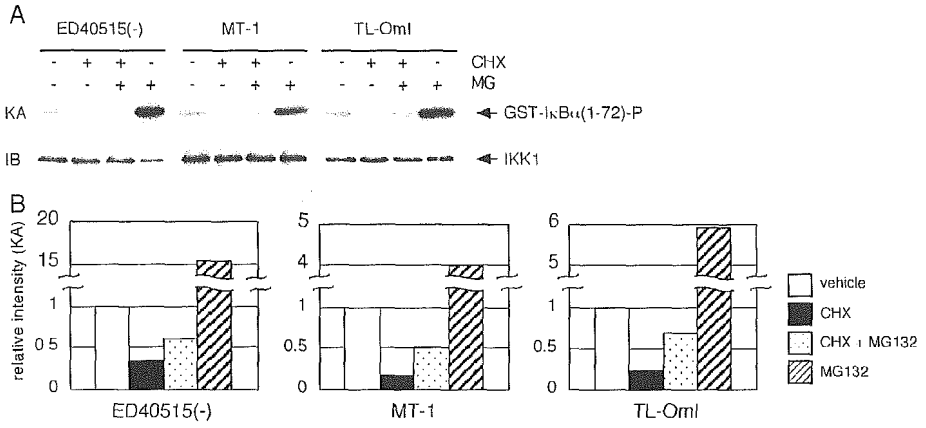

Fig. 2. Pretreatment with MG132 reverses the CHX-mediated IKK inhibition. (A) ATL cells were treated with vehicle (DMSO) or MG132 (20 μM) for 30 min before addition of vehicle (H_2O) or CHX (50 μg/ml). After 4 h of incubation, cytoplasmic extracts (600 μg) were subjected to immunoprecipitation with NEMO antiserum. Immunoprecipitates were used for in vitro kinase assay (KA) and detection of IKK1 by immunoblotting (IB). (B) Relative band intensity of phosphorylated GST-IκBα (1–72) was normalized to the corresponding immunoprecipitated IKK1 band intensity. A value of 1.0 represents normalized phosphorylated GST-IκBα (1–72) band intensity obtained in each control experiment: open bar, vehicle control; closed bar, 50 μg/ml cycloheximide; dotted bar, 50 μg/ml cycloheximide + 20 μM MG132; scratched bar, 20 μM MG132. The experiments were carried out at least three times and the results were essentially reproducible.

with a previous report [40], 8 h of arsenite treatment impaired Tax expression in MT-2 cells, but not in HUT-102 or SLB-1 cells in our experimental condition (Fig. 4C). We therefore asked if arsenite-induced reduction in Tax expression is primarily responsible for down-regulation of IKK activity. IKK activity in Tax-positive HTLV-I-transformed cells declined as soon as 1 h after treatment with arsenite in a dose-dependent manner (Figs. 5A and B); however, Tax expression was not affected at this time point (Fig. 5C). Thus, at 1 h after treatment, down-regulation of IKK activity

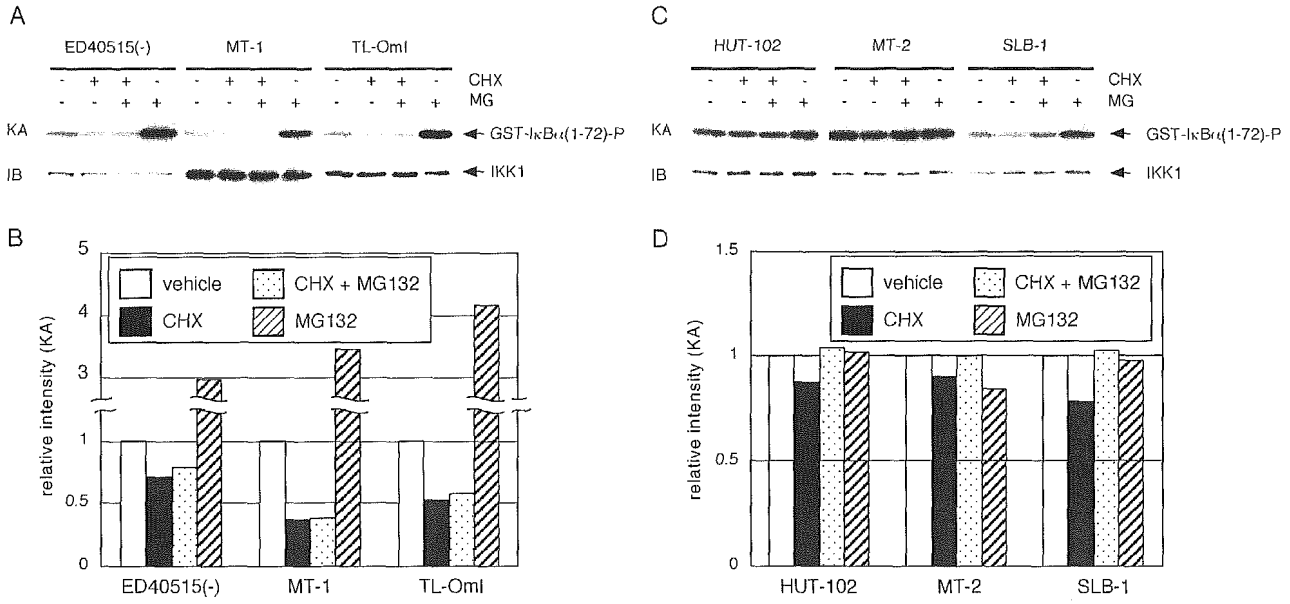

Fig. 3. MG132 does not restore IKK activity after CHX treatment in ATL cells. (A) ATL cells were treated with vehicle (H_2O) or CHX (50 μg/ml) for 1 h before addition of vehicle (DMSO) or MG132 (20 μM). After 3 h of incubation, cytoplasmic extracts (600 μg) were subjected to immunoprecipitation with NEMO antiserum, and immunoprecipitates were used for in vitro kinase assay (KA) and detection of IKK1 by immunoblotting (IB). (B) Relative band intensity of phosphorylated GST-IκBα (1–72) was normalized to the corresponding immunoprecipitated IKK1 band intensity. A value of 1.0 represents normalized phosphorylated GST-IκBα (1–72) band intensity obtained in each control experiment: open bar, vehicle control; closed bar, 50 μg/ml cycloheximide; dotted bar, 50 μg/ml cycloheximide + 20 μM MG132; scratched bar, 20 μM MG132. (C) HTLV-I-transformed cells were treated with vehicle (H_2O) or CHX (50 μg/ml) for 1 h before addition of vehicle (DMSO) or MG132 (20 μM). After 3 h of incubation, cytoplasmic extracts (600 μg) were subjected to immunoprecipitation with NEMO antiserum, and immunoprecipitates were used for in vitro kinase assay (KA) and detection of IKK1 by immunoblotting (IB). (D) Relative band intensity of phosphorylated GST-IκBα (1–72) was normalized to the corresponding immunoprecipitated IKK1 band intensity. A value of 1.0 represents normalized phosphorylated GST-IκBα (1–72) band intensity obtained in each control experiment: open bar, vehicle control; closed bar, 50 μg/ml cycloheximide; dotted bar, 50 μg/ml cycloheximide + 20 μM MG132; scratched bar, 20 μM MG132. The experiments were carried out at least three times and the results were essentially reproducible.

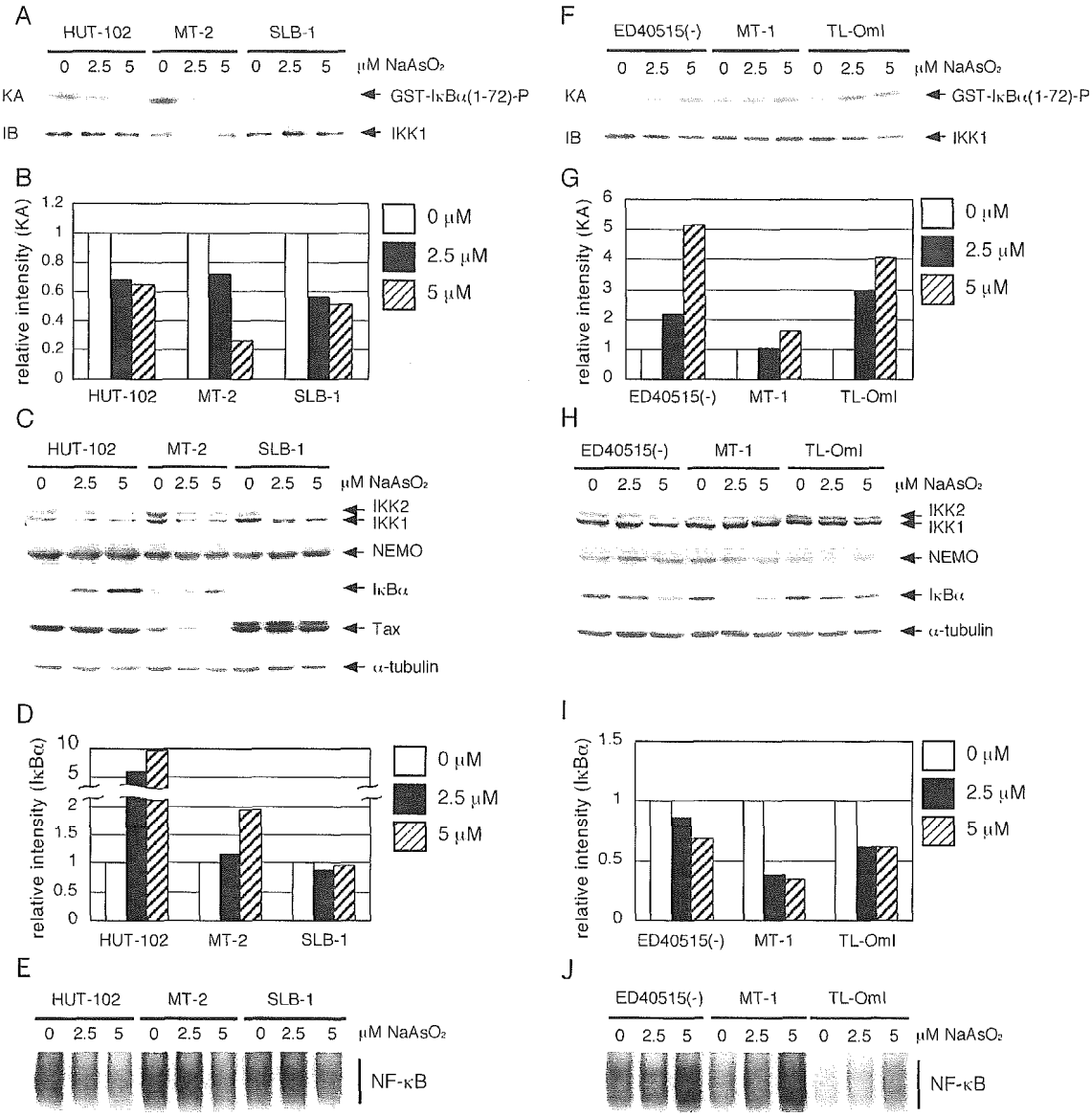

Fig. 4. Arsenite treatment does not impair IKK activity in ATL cells. (A) HTLV-I-transformed cells were treated with RPMI or the indicated concentrations of sodium arsenite for 8 h. Cytoplasmic extracts (600 μg) were subjected to immunoprecipitation with NEMO antiserum, and immunoprecipitates were used for in vitro kinase assay (KA) and detection of IKK1 by immunoblotting (IB). (B) Relative band intensity of phosphorylated GST-IκBα (1–72) was normalized to the corresponding immunoprecipitated IKK1 band intensity. A value of 1.0 represents normalized phosphorylated GST-IκBα (1–72) band intensity in the absence of arsenite (0 μM): open bar, 0 μM; closed bar, 2.5 μM; scratched bar, 5 μM. (C) Whole cell extracts (50 μg) were separated on SDS-polyacrylamide gel and subjected to immunoblotting. IKK1, IKK2, NEMO, IκBα, Tax, and α-tubulin were detected by immunoblotting. (D) Relative band intensity of IκBα was normalized to the corresponding α-tubulin band intensity. A value of 1.0 represents normalized IκBα band intensity in the absence of arsenite (0 μM): open bar, 0 μM; closed bar, 2.5 μM; scratched bar, 5 μM. (E) HTLV-I-transformed cells were treated for 12 h with RPMI or the indicated concentrations of sodium arsenite. One microgram of nuclear extracts from the indicated cell lines were analyzed by EMSA using the ^{32}P-labeled κB probe. (F) ATL cells were treated with RPMI or the indicated concentrations of sodium arsenite for 8 h. Cytoplasmic extracts (600 μg) were subjected to immunoprecipitation with NEMO antiserum, and immunoprecipitates were used for in vitro kinase assay (KA) and detection of IKK1 by immunoblotting (IB). (G) Relative band intensity of phosphorylated GST-IκBα (1–72) was normalized to the corresponding immunoprecipitated IKK1 band intensity. A value of 1.0 represents normalized phosphorylated GST-IκBα (1–72) band intensity in the absence of arsenite (0 μM): open bar, 0 μM; closed bar, 2.5 μM; scratched bar, 5 μM. (H) Whole cell extracts (50 μg) were separated on SDS-polyacrylamide gel and subjected to immunoblotting for detection of IKK1, IKK2, NEMO, IκBα, and α-tubulin. (I) Relative band intensity of IκBα was normalized to the corresponding α-tubulin band intensity. A value of 1.0 represents normalized IκBα band intensity in the absence of arsenite (0 μM): open bar, 0 μM; closed bar, 2.5 μM; scratched bar, 5 μM. (J) ATL cells were treated for 12 h with RPMI or the indicated concentrations of sodium arsenite. Nuclear extracts (3 μg) from the indicated cell lines were analyzed by EMSA using the ^{32}P-labeled κB probe. The experiments were carried out at least three times and the results were essentially reproducible.

by arsenite was not due to reduced expression of Tax. On the other hand, this brief arsenite treatment did not change IKK activity in ATL cells except for ED40515(−) cells (Figs. 5F and G). Equivalent amounts of the IKK components were present in ATL cells under this condition (Figs. 5C and H). This treatment might be too short to

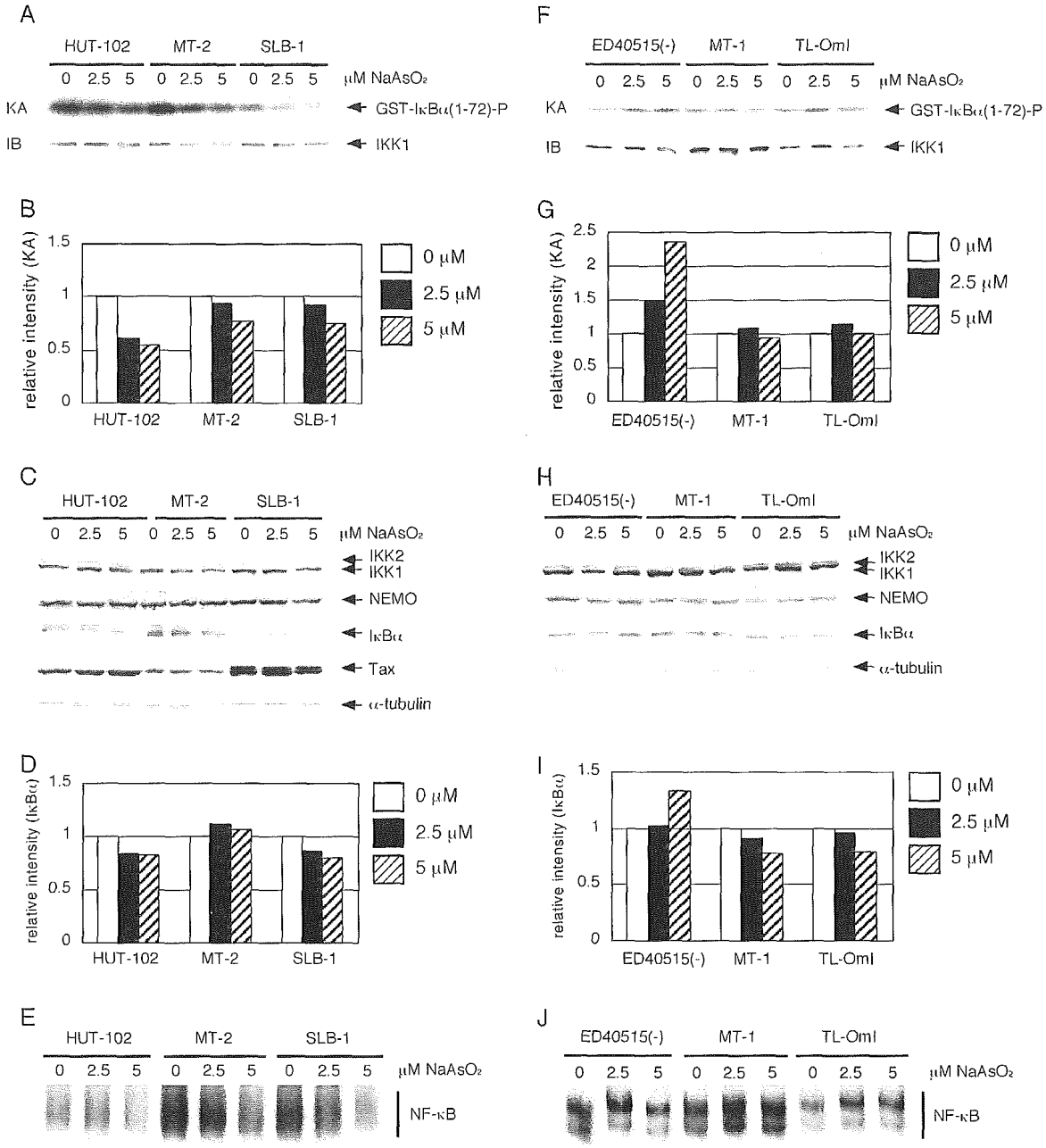

Fig. 5. Arsenite down-regulates IKK activity in HTLV-I-transformed cells without affecting Tax expression. (A) HTLV-I-transformed cells were treated with vehicle (RPMI) or the indicated concentrations of sodium arsenite for 1 h. Cytoplasmic extracts (600 μg) were subjected to immunoprecipitation with NEMO antiserum, and immunoprecipitates were used for in vitro kinase assay (KA) and detection of IKK1 by immunoblotting (IB). (B) Relative band intensity of phosphorylated GST-IκBα (1–72) was normalized to the corresponding immunoprecipitated IKK1 band intensity. A value of 1.0 represents normalized phosphorylated GST-IκBα (1–72) band intensity in the absence of arsenite (0 μM): open bar, 0 μM; closed bar, 2.5 μM; scratched bar, 5 μM. (C) Whole cell extracts (50 μg) were resolved by SDS-polyacrylamide gel electrophoresis and subjected to immunoblotting for detection of IKK1, IKK2, NEMO, Tax, and α-tubulin. (D) Relative band intensity of IκBα was normalized to the corresponding α-tubulin band intensity. A value of 1.0 represents normalized IκBα band intensity in the absence of arsenite (0 μM): open bar, 0 μM; closed bar, 2.5 μM; scratched bar, 5 μM. (E) HTLV-I-transformed cells were treated with RPMI or the indicated concentrations of sodium arsenite for 2 h. Nuclear extracts (1 μg) from the indicated cell lines were analyzed by EMSA using the ^{32}P-labeled κB probe. (F) ATL cells were treated with vehicle (RPMI) or the indicated concentrations of sodium arsenite for 1 h. Cytoplasmic extracts (600 μg) were subjected to immunoprecipitation with NEMO antiserum, and immunoprecipitates were used for in vitro kinase assay (KA) and detection of IKK1 by immunoblotting (IB). (G) Relative band intensity of phosphorylated GST-IκBα (1–72) was normalized to the corresponding immunoprecipitated IKK1 band intensity. A value of 1.0 represents normalized phosphorylated GST-IκBα (1–72) band intensity in the absence of arsenite (0 μM): open bar, 0 μM; closed bar, 2.5 μM; scratched bar, 5 μM. (H) Whole cell extracts (50 μg) were separated on SDS-polyacrylamide gel and subjected to immunoblotting for detection of IKK1, IKK2, NEMO, and α-tubulin. (I) Relative band intensity of IκBα was normalized to the corresponding α-tubulin band intensity. A value of 1.0 represents normalized IκBα band intensity in the absence of arsenite (0 μM): open bar, 0 μM; closed bar, 2.5 μM; scratched bar, 5 μM. (J) ATL cells were treated with RPMI or the indicated concentrations of sodium arsenite for 2 h. Nuclear extracts (3 μg) from the indicated cell lines were analyzed by EMSA using the ^{32}P-labeled κB probe. The experiments were carried out at least three times and the results were essentially reproducible.

apparently alter the steady-state levels of IκBα and DNA binding activity (Figs. 5D, E, I, and J).

Discussion

A number of papers, reviewed in references [41–44], have demonstrated constitutive NF-κB activation in a wide range of human malignancies, most of them dealing with NF-κB DNA binding activity and/or the status of IκB proteins. Few reports examined IKK activity in cancer cells [45–54], among which only three papers investigated a mechanism of IKK activation. Constitutive activation of Bcr-Abl or Akt was implicated in NF-κB activation in chronic myeloid leukemia [55] and colorectal cancer [56], respectively, but how these kinases are linked to IKK remained to be clarified.

In the field of HTLV-I research, the differences between Tax-induced and Tax-independent NF-κB activation in HTLV-I-infected T cells have not been well recognized. Many reports described that c-Rel was induced by Tax and constituted the DNA binding activity in T lymphocytes [57–60]. In contrast, Mori et al. demonstrated that the DNA binding complexes in primary ATL cells are predominantly comprised of p50 and RelA [6]. Hironaka et al. demonstrated a Tax-independent constitutive IKK activation in ATL cells that was suppressed by a dominant-negative form of IKK1/α, but not by that of IKK2/β or NEMO, suggesting an involvement of the non-canonical pathway of NF-κB activation [29]. However, it remained unknown what differences in the upstream regulatory mechanism determine the distinct IKK activation and NF-κB components. We now demonstrate for the first time that the IKK activity in Tax-positive and -negative HTLV-I-infected cells is differentially modulated by treatment with a protein synthesis inhibitor cycloheximide, a proteasome inhibitor MG132, or arsenite.

While previous studies demonstrated that CHX blocked signal-induced processing of p100 [23,24,26,27], the regulatory effects of CHX on IKK activity or p100 processing in tumor cells remained to be studied. This prompted us to examine if IKK activity in ATL cells is affected by CHX. The rapid down-regulation of IKK activity in ATL cells treated with CHX (Fig. 1), combined with their aberrant p52 expression, strongly suggests that the non-canonical NF-κB activation pathway is usurped in ATL cells. Regarding the constitutive IKK activity in tumor cells, this is the first report demonstrating that it is lost quickly after protein synthesis inhibition in ATL cells. CHX has similar inhibitory effect on IKK activity in other types of tumor cells characterized by constitutive NF-κB activity (unpublished observation).

Proteasome inhibitors have recently emerged as an interesting and potentially new group of chemotherapeutic agents for a variety of human cancers which have constitutively activated NF-κB activity, including squamous cell carcinoma [61], colorectal cancer [62], acute myelogenous leukemia [63], multiple myeloma [64], and mantle cell lymphoma [65]. Proteasome inhibitors act as a stabilizer for IκB proteins, resulting in inhibition of NF-κB activity. However, there has been no report on its effect on IKK activity in tumor cells except for one paper describing elevated IKK activity following MG132 treatment of a colon cancer cell line HT-29 [66]. Inhibiting NF-κB activation in these cells prevents tumor cell growth and finally induces apoptosis. Mori et al. demonstrated that inhibition of constitutive NF-κB induced apoptosis of primary ATL cells [67,68]. Thus, proteasome inhibitors are potentially effective on ATL. On the other hand, the remarkable enhancement of IKK activity in ATL cells after treatment with a proteasome inhibitor MG132 has uncovered another role of proteasome, regulation of IKK activity. In this regard, Liao et al. recently demonstrated that TRAF3 interacted with NIK and promoted poly-ubiquitination and proteasome-dependent degradation of NIK, thereby inhibiting NIK-induced p100 processing [69]. We have demonstrated in this report that proteasome inhibition strongly enhances IKK activity in ATL cells that aberrantly express p52 [29], implicating that NIK may contribute to IKK activation in ATL cells. This also suggests that NIK is unlikely to evade the TRAF3 regulation in ATL cells, because IKK activity is still under the control of the proteasome. Indeed, the steady-state levels of TRAF3 in ATL cells were comparable to those in other T cell lines (data not shown). We attempted to determine whether NIK is activated in ATL cells by in vitro kinase assay coupled with immunoprecipitation of NIK, but failed to detect NIK and could not find any autophosphorylation of NIK that was easily detected following transient overexpression of NIK in 293T cells (data not shown). Nevertheless, accumulating evidence on the TNF receptor family members that transduce signals leading to p100 processing raises a possibility that ATL cells may aberrantly express one or more of this family members. For instance, Uchiyama et al. demonstrated that ATL cells showed adhesion to vascular endothelial cells through OX40/gp34 interaction [70,71]. They also reported that activation of OX40 signaling in ATL cells attenuated Fas-induced apoptosis [72]. These results suggested that OX40 contributed to survival and expansion of leukemic cells in ATL patients. Although OX40 is often found to be expressed in freshly isolated ATL cells and reported to contribute to tumor cell adhesion [73], its contribution to NF-κB activation in ATL cells remains to be studied. On the other hand, CD30 is expressed only in a small fraction of ATL cells that show anaplastic large cell leukemia-like morphology [74]. Further efforts will be required to clarify the cause of constitutive IKK activation in ATL cells.

Kapahi et al. previously reported that arsenite, at relatively high concentrations, inhibited IKK activity induced by TNF-α, NIK overexpression or a constitutively active form of IKK2 expressed in HeLa cells [39]. They

clearly demonstrated that the cysteine residue in the activation loop of IKK2 was the direct target for inhibition by arsenite. We have demonstrated here that arsenite rapidly down-regulates constitutive IKK activity in HTLV-I-transformed cells without appreciable decrease in Tax expression at clinically relevant concentrations. The result that IKK activity of ATL cells was not impaired at least up to 8 h after treatment with arsenite may suggest a mutation in the cysteine residue, but sequence analysis of IKK cDNAs from ED40515(−), MT-1, and TL-OmI cells revealed that the amino acid alignment of IKK in the activation loop remained intact (data not shown). Bazarbachi et al. reported that a combination treatment of arsenic trioxide and interferon α (IFN-α) induced down-regulation of Tax expression, impaired degradation of IκB proteins and reduced DNA binding activity, which eventually led to apoptosis of HTLV-I-transformed cells [40]. They also showed that IKK activity was not affected by arsenic alone or arsenic with IFN-α [75]. While Bazarbachi et al. observed effects of arsenic at 1 μM, we used arsenite at 2.5 to 5 μM, which inhibited IKK activity prior to down-regulation of Tax expression (Fig. 5). The differences in concentration and compound might explain the discrepancy between the results. Arsenic and arsenite are reported to induce apoptosis of a variety of cancer cells including acute promyelocytic leukemia [76], neuroblastoma [77], breast cancer [78], renal cell carcinoma [79], multiple myeloma [80], cutaneous T cell lymphoma [81], Hodgkin/Reed-Sternberg (H-RS) cell [82], and Bcr-Abl-positive leukemia [83]. These reports showed that arsenic induced down-regulation of Bcl-2 [76,77,80], Bcl-XL [79] or Bcr-Abl expression [83], up-regulation of p53 expression [78], or reduction of CDK6 and hypophosphorylation of pRb protein [79,80]. In addition, Ivanov et al. showed that arsenite down-regulated NF-κB activity and induced TNF-α-mediated apoptosis in multiple myeloma cells [84]. Mathas et al. demonstrated that arsenite inhibition of constitutive IKK activity induced apoptosis in H-RS cells [82]. While IKK activity in ATL cells seemed weakly enhanced 8 h after arsenite treatment (Fig. 4), incubation with arsenite for 24 h induced down-regulation of IKK activity and cell death in ATL and HTLV-I-transformed cells (data not shown). Nevertheless, the differential responses of ATL and HTLV-I-transformed cells to the arsenite treatments implicate distinct mechanisms of IKK activation in these cells.

In conclusion, our results indicate that IKK activity is differentially regulated in ATL and Tax-positive HTLV-I-transformed cells. Previous studies on Tax indeed have provided invaluable insight into NF-κB signaling [18] and cell transformation, but events caused by Tax may not be of great help for further studies on ATL cells. Instead, identification of a labile factor responsible for IKK activation in the absence of Tax and understanding the mechanism by which this factor contributes to the constitutive IKK activity in ATL cells will facilitate establishing a novel therapeutic strategy not only against ATL, but also against other neoplastic disorders characterized by constitutive NF-κB activation.

Acknowledgments

We thank Dr. Gilles Courtois (Hopital Saint-Louis, Paris), Dr. Anning Lin (University of Chicago, IL), Dr. Hiroyasu Nakano (Juntendo University, Tokyo), and the members of the Department of Molecular Virology, Tokyo Medical and Dental University for helpful discussion and comments. This work was supported by Grant-in-Aid for Scientific Research on Priority Areas from the Ministry of Education, Culture, Sports, Science and Technology to N.Y. and S.Y., grant from the Ministry of Health, Labor and Welfare of Japan and the Human Science Foundation to N.Y., and Grant-in-Aid for Scientific Research (C) from the Ministry of Education, Culture, Sports, Science and Technology to S.Y.

References

[1] T. Uchiyama, J. Yodoi, K. Sagawa, K. Takatsuki, H. Uchino, Adult T-cell leukemia: clinical and hematologic features of 16 cases, Blood 50 (1977) 481–492.
[2] K. Takahashi, T. Uchiyama, Y. Ueshima, T. Hattori, Adult T-cell leukemia: further clinical observations and cytogenic and functional studies of leukemic cells, Jpn. J. Clin. Oncol. 9 (Suppl.) (1979) 317–324.
[3] Y. Hinuma, K. Nagata, M. Hanaoka, M. Nakai, M. Matsumoto, K.I. Kinoshita, S. Shirakawa, I. Miyoshi, Adult T-cell leukemia: antigen in an ATL cell line and detection of antibodies to the antigen in human sera, Proc. Natl. Acad. Sci. U. S. A. 78 (1981) 6476–6480.
[4] M. Yoshida, I. Miyoshi, Y. Hinuma, Isolation and characterization of retrovirus from cell lines of human adult T-cell leukemia and its implication in the disease, Proc. Natl. Acad. Sci. U. S. A. 79 (1982) 2031–2035.
[5] K. Tajima, S. Tominaga, T. Suchi, T. Kawagoe, H. Komoda, Y. Hinuma, T. Oda, K. Fujita, Epidemiological analysis of the distribution of antibody to adult T-cell leukemia-virus-associated antigen: possible horizontal transmission of adult T-cell leukemia virus, Gann 73 (1982) 893–901.
[6] N. Mori, M. Fujii, S. Ikeda, Y. Yamada, M. Tomonaga, D.W. Ballard, N. Yamamoto, Constitutive activation of NF-kappaB in primary adult T-cell leukemia cells, Blood 93 (1999) 2360–2368.
[7] N. Mori, M. Fujii, K. Iwai, S. Ikeda, Y. Yamasaki, T. Hata, Y. Yamada, Y. Tanaka, M. Tomonaga, N. Yamamoto, Constitutive activation of transcription factor AP-1 in primary adult T-cell leukemia cells, Blood 95 (2000) 3915–3921.
[8] M. Karin, Y. Ben-Neriah, Phosphorylation meets ubiquitination: the control of NF-kappaB activity, Annu. Rev. Immunol. 18 (2000) 621–663.
[9] X. Li, G.R. Stark, NF-kappaB-dependent signaling pathways, Exp. Hematol. 30 (2002) 285–296.
[10] S.C. Sun, G. Xiao, Deregulation of NF-kappaB and its upstream kinases in cancer, Cancer Metastasis Rev. 22 (2003) 405–422.
[11] R. Horie, M. Higashihara, T. Watanabe, Hodgkin's lymphoma and CD30 signal transduction, Int. J. Hematol. 77 (2003) 37–47.
[12] M. Karin, Y. Cao, F.R. Greten, Z.W. Li, NF-kappaB in cancer: from innocent bystander to major culprit, Nat. Rev. 2 (2002) 301–310.

[13] S. Ghosh, M.J. May, E.B. Kopp, NF-kappaB and rel proteins: evolutionarily conserved mediators of immune responses, Annu. Rev. Immunol. 16 (1998) 225–260.
[14] Z.J. Chen, L. Parent, T. Maniatis, Site-specific phosphorylation of IkappaBalpha by a novel ubiquitination-dependent protein kinase activity, Cell 84 (1996) 853–862.
[15] J.A. DiDonato, M. Hayakawa, D.M. Rothwarf, E. Zandi, M. Karin, A cytokine-responsive IkappaB kinase that activates the transcription factor NF-kappaB, Nature 388 (1997) 548–554.
[16] F. Mercurio, H. Zhu, B.W. Murray, A. Shevchenko, B.L. Bennett, J. Li, D.B. Young, M. Barbosa, M. Mann, A. Manning, A. Rao, IKK-1 and IKK-2: cytokine-activated IkappaB kinases essential for NF-kappaB activation, Science 278 (1997) 860–866.
[17] E. Zandi, D.M. Rothwarf, M. Delhase, M. Hayakawa, M. Karin, The IkappaB kinase complex (IKK) contains two kinase subunits, IKKalpha and IKKbeta, necessary for IkappaB phosphorylation and NF-kappaB activation, Cell 91 (1997) 243–252.
[18] S. Yamaoka, G. Courtois, C. Bessia, S.T. Whiteside, R. Weil, F. Agou, H.E. Kirk, R.J. Kay, A. Israel, Complementation cloning of NEMO, a component of the IkappaB kinase complex essential for NF-kappaB activation, Cell 93 (1998) 1231–1240.
[19] D.M. Rothwarf, E. Zandi, G. Natoli, M. Karin, IKK-gamma is an essential regulatory subunit of the IkappaB kinase complex, Nature 395 (1998) 297–300.
[20] A. Matsushima, T. Kaisho, P.D. Rennert, H. Nakano, K. Kurosawa, D. Uchida, K. Takeda, S. Akira, M. Matsumoto, Essential role of nuclear factor (NF)-kappaB-inducing kinase and inhibitor of kappaB (IkappaB) kinase alpha in NF-kappaB activation through lymphotoxin beta receptor, but not through tumor necrosis factor receptor I, J. Exp. Med. 193 (2001) 631–636.
[21] T. Saitoh, H. Nakano, N. Yamamoto, S. Yamaoka, Lymphotoxin-beta receptor mediates NEMO-independent NF-kappaB activation, FEBS Lett. 532 (2002) 45–51.
[22] E. Dejardin, N.M. Droin, M. Delhase, E. Haas, Y. Cao, C. Makris, Z.W. Li, M. Karin, C.F. Ware, D.R. Green, The lymphotoxin-beta receptor induces different patterns of gene expression via two NF-kappaB pathways, Immunity 17 (2002) 525–535.
[23] J.R. Muller, U. Siebenlist, Lymphotoxin beta receptor induces sequential activation of distinct NF-kappa B factors via separate signaling pathways, J. Biol. Chem. 278 (2003) 12006–12012.
[24] E. Claudio, K. Brown, S. Park, H. Wang, U. Siebenlist, BAFF-induced NEMO-independent processing of NF-kappa B2 in maturing B cells, Nat. Immunol. 3 (2002) 958–965.
[25] N. Kayagaki, M. Yan, D. Seshasayee, H. Wang, W. Lee, D.M. French, I.S. Grewal, A.G. Cochran, N.C. Gordon, J. Yin, M.A. Starovasnik, V.M. Dixit, BAFF/BLyS receptor 3 binds the B cell survival factor BAFF ligand through a discrete surface loop and promotes processing of NF-kappaB2, Immunity 17 (2002) 515–524.
[26] T. Saitoh, M. Nakayama, H. Nakano, H. Yagita, N. Yamamoto, S. Yamaoka, TWEAK induces NF-kappaB2 p100 processing and long lasting NF-kappaB activation, J. Biol. Chem. 278 (2003) 36005–36012.
[27] H.J. Coope, P.G. Atkinson, B. Huhse, M. Belich, J. Janzen, M.J. Holman, G.G. Klaus, L.H. Johnston, S.C. Ley, CD40 regulates the processing of NF-kappaB2 p100 to p52, EMBO J. 21 (2002) 5375–5385.
[28] G. Xiao, M.E. Cvijic, A. Fong, E.W. Harhaj, M.T. Uhlik, M. Waterfield, S.C. Sun, Retroviral oncoprotein Tax induces processing of NF-kappaB2/p100 in T cells: evidence for the involvement of IKKalpha, EMBO J. 20 (2001) 6805–6815.
[29] N. Hironaka, K. Mochida, N. Mori, M. Maeda, N. Yamamoto, S. Yamaoka, Tax-independent constitutive IkappaB kinase activation in adult T-cell leukemia cells, Neoplasia 6 (2004) 266–278.
[30] M. Maeda, A. Shimizu, K. Ikuta, H. Okamoto, M. Kashihara, T. Uchiyama, T. Honjo, J. Yodoi, Origin of human T-lymphotrophic virus I-positive T cell lines in adult T cell leukemia. Analysis of T cell receptor gene rearrangement, J. Exp. Med. 162 (1985) 2169–2174.
[31] I. Miyoshi, I. Kubonishi, M. Sumida, S. Hiraki, T. Tsubota, I. Kimura, K. Miyamoto, J. Sato, A novel T-cell line derived from adult T-cell leukemia, Gann 71 (1980) 155–156.
[32] K. Sugamura, M. Fujii, M. Kannagi, M. Sakitani, M. Takeuchi, Y. Hinuma, Cell surface phenotypes and expression of viral antigens of various human cell lines carrying human T-cell leukemia virus, Int. J. Cancer 34 (1984) 221–228.
[33] B.J. Poiesz, F.W. Ruscetti, A.F. Gazdar, P.A. Bunn, J.D. Minna, R.C. Gallo, Detection and isolation of type C retrovirus particles from fresh and cultured lymphocytes of a patient with cutaneous T-cell lymphoma, Proc. Natl. Acad. Sci. U. S. A. 77 (1980) 7415–7419.
[34] I. Miyoshi, I. Kubonishi, S. Yoshimoto, T. Akagi, Y. Ohtsuki, Y. Shiraishi, K. Nagata, Y. Hinuma, Type C virus particles in a cord T-cell line derived by co-cultivating normal human cord leukocytes and human leukaemic T cells, Nature 294 (1981) 770–771.
[35] H.P. Koeffler, I.S. Chen, D.W. Golde, Characterization of a novel HTLV-infected cell line, Blood 64 (1984) 482–490.
[36] K. Mori, H. Sabe, H. Siomi, T. Iino, A. Tanaka, K. Takeuchi, K. Hirayoshi, M. Hatanaka, Expression of a provirus of human T cell leukaemia virus type I by DNA transfection, J. Gen. Virol. 68 (1987) 499–506.
[37] N. Chinanonwait, H. Miura, N. Yamamoto, S. Yamaoka, A recessive mutant cell line with a constitutive IkappaB kinase activity, FEBS Lett. 531 (2002) 553–560.
[38] M. Kieran, V. Blank, F. Logeat, J. Vandekerckhove, F. Lottspeich, O. Le Bail, M.B. Urban, P. Kourilsky, P.A. Baeuerle, A. Israel, The DNA binding subunit of NF-kappa B is identical to factor KBF1 and homologous to the rel oncogene product, Cell 62 (1990) 1007–1018.
[39] P. Kapahi, T. Takahashi, G. Natoli, S.R. Adams, Y. Chen, R.Y. Tsien, M. Karin, Inhibition of NF-kappa B activation by arsenite through reaction with a critical cysteine in the activation loop of Ikappa B kinase, J. Biol. Chem. 275 (2000) 36062–36066.
[40] M.E. El-Sabban, R. Nasr, G. Dbaibo, O. Hermine, N. Abboushi, F. Quignon, J.C. Ameisen, F. Bex, H. de The, A. Bazarbachi, Arsenic-interferon-alpha-triggered apoptosis in HTLV-I transformed cells is associated with Tax down-regulation and reversal of NF-kappa B activation, Blood 96 (2000) 2849–2855.
[41] M. Karin, Y. Cao, F.R. Greten, Z.W. Li, NF-kappaB in cancer: from innocent bystander to major culprit, Nat. Rev., Cancer 2 (2002) 301–310.
[42] A.S. Baldwin, Control of oncogenesis and cancer therapy resistance by the transcription factor NF-kappaB, J. Clin. Invest. 107 (2001) 241–246.
[43] B.B. Aggarwal, Nuclear factor-kappaB: the enemy within, Cancer Cell 6 (2004) 203–208.
[44] S.C. Sun, G. Xiao, Deregulation of NF-kappaB and its upstream kinases in cancer, Cancer Metastasis Rev. 22 (2003) 405–422.
[45] T. Syrovets, J.E. Gschwend, B. Buchele, Y. Laumonnier, W. Zugmaier, F. Genze, T. Simmet, Inhibition of IκB kinase activity by acetyl-boswellic acids promotes apoptosis in androgen-independent PC-3 prostate cancer cells in vitro and in vivo, J. Biol. Chem. 280 (2005) 6170–6180.
[46] M. Broemer, D. Krappmann, C. Scheidereit, Requirement of Hsp90 activity for IkappaB kinase (IKK) biosynthesis and for constitutive and inducible IKK and NF-kappaB activation, Oncogene 23 (2004) 5378–5386.
[47] R.E. Davis, K.D. Brown, U. Siebenlist, L.M. Staudt, Constitutive nuclear factor kappaB activity is required for survival of activated B cell-like diffuse large B cell lymphoma cells, J. Exp. Med. 194 (2001) 1861–1874.
[48] J. Yang, A. Richmond, Constitutive IkappaB kinase activity correlates with nuclear factor-kappaB activation in human melanoma cells, Cancer Res. 61 (2001) 4901–4909.
[49] A.V. Gasparian, Y.J. Yao, D. Kowalczyk, L.A. Lyakh, A. Karseladze, T.J. Slaga, I.V. Budunova, The role of IKK in constitutive activation of NF-kappaB transcription factor in prostate carcinoma cells, J. Cell Sci. 115 (2002) 141–151.

[50] R. Romieu-Mourez, E. Landesman-Bollag, D.C. Seldin, A.M. Traish, F. Mercurio, G.E. Sonenshein, Roles of IKK kinases and protein kinase CK2 in activation of nuclear factor-kappaB in breast cancer, Cancer Res. 61 (2001) 3810–3818.

[51] B. Baumgartner, M. Weber, M. Quirling, C. Fischer, S. Page, M. Adam, C. Von Schilling, C. Waterhouse, C. Schmid, D. Neumeier, K. Brand, Increased IkappaB kinase activity is associated with activated NF-kappaB in acute myeloid blasts, Leukemia 16 (2002) 2062–2071.

[52] G. Munzert, D. Kirchner, O. Ottmann, L. Bergmann, R.M. Schmid, Constitutive NF-kappab/Rel activation in philadelphia chromosome positive (Ph+) acute lymphoblastic leukemia (ALL), Leuk. Lymphoma 45 (2004) 1181–1184.

[53] T. Tamatani, M. Azuma, K. Aota, T. Yamashita, T. Bando, M. Sato, Enhanced IkappaB kinase activity is responsible for the augmented activity of NF-kappaB in human head and neck carcinoma cells, Cancer Lett. 171 (2001) 165–172.

[54] L. Ludwig, H. Kessler, M. Wagner, C. Hoang-Vu, H. Dralle, G. Adler, B.O. Bohm, R.M. Schmid, Nuclear factor-kappaB is constitutively active in C-cell carcinoma and required for RET-induced transformation, Cancer Res. 61 (2001) 4526–4535.

[55] D. Kirchner, J. Duyster, O. Ottmann, R.M. Schmid, L. Bergmann, G. Munzert, Mechanisms of Bcr-Abl-mediated NF-kappaB/Rel activation, Exp. Hematol. 31 (2003) 504–511.

[56] A. Agarwal, K. Das, N. Lerner, S. Sathe, M. Cicek, G. Casey, N. Sizemore, The AKT/I kappa B kinase pathway promotes angiogenic/metastatic gene expression in colorectal cancer by activating nuclear factor-kappa B and beta-catenin, Oncogene 24 (2005) 1021–1031.

[57] N. Arima, J.A. Molitor, M.R. Smith, J.H. Kim, Y. Daitoku, W.C. Greene, Human T-cell leukemia virus type I Tax induces expression of the Rel-related family of kappa B enhancer-binding proteins: evidence for a pretranslational component of regulation, J. Virol. 65 (1991) 6892–6899.

[58] I. Crenon, C. Beraud, P. Simard, J. Montagne, P. Veschambre, P. Jalinot, Related articles, links abstract. The transcriptionally active factors mediating the effect of the HTLV-I Tax transactivator on the IL-2R alpha kappa B enhancer include the product of the c-rel proto-oncogene, Oncogene 8 (1993) 867–875.

[59] N. Pepin, A. Roulston, J. Lacoste, R. Lin, J. Hiscott, Subcellular redistribution of HTLV-1 Tax protein by NF-kappa B/Rel transcription factors, Virology 204 (1994) 706–716.

[60] J. Lanoix, J. Lacoste, N. Pepin, N. Rice, J. Hiscott, Overproduction of NFKB2 (lyt-10) and c-Rel: a mechanism for HTLV-I Tax-mediated trans-activation via the NF-kappa B signalling pathway, Oncogene 9 (1994) 841–852.

[61] J.B. Sunwoo, Z. Chen, G. Dong, N. Yeh, C.C. Bancroft, E. Sausville, J. Adams, P. Elliott, C. Van Waes, Novel proteasome inhibitor PS-341 inhibits activation of nuclear factor-kappa B, cell survival, tumor growth, and angiogenesis in squamous cell carcinoma, Clin. Cancer Res. 7 (2001) 1419–1428.

[62] D.S. Lind, S.N. Hochwald, J. Malaty, S. Rekkas, P. Hebig, G. Mishra, L.L. Moldawer, E.M. Copeland III, S. Mackay, Nuclear factor-kappa B is upregulated in colorectal cancer, Surgery 130 (2001) 363–369.

[63] M.L. Guzman, S.J. Neering, D. Upchurch, B. Grimes, D.S. Howard, D.A. Rizzieri, S.M. Luger, C.T. Jordan, Nuclear factor-kappaB is constitutively activated in primitive human acute myelogenous leukemia cells, Blood 98 (2001) 2301–2307.

[64] H. Ni, M. Ergin, Q. Huang, J.Z. Qin, H.M. Amin, R.L. Martinez, S. Saeed, K. Barton, S. Alkan, Analysis of expression of nuclear factor kappa B (NF-kappa B) in multiple myeloma: downregulation of NF-kappa B induces apoptosis, Br. J. Haematol. 115 (2001) 279–286.

[65] L.V. Pham, A.T. Tamayo, L.C. Yoshimura, P. Lo, R.J. Ford, Inhibition of constitutive NF-kappa B activation in mantle cell lymphoma B cells leads to induction of cell cycle arrest and apoptosis, J. Immunol. 171 (2003) 88–95.

[66] Z.H. Nemeth, H.R. Wong, K. Odoms, E.A. Deitch, C. Szabo, E.S. Vizi, G. Hasko, Proteasome inhibitors induce inhibitory kappa B (I kappa B) kinase activation, I kappa B alpha degradation, and nuclear factor kappa B activation in HT-29 cells, Mol. Pharmacol. 65 (2004) 342–349.

[67] N. Mori, Y. Yamada, S. Ikeda, Y. Yamasaki, K. Tsukasaki, Y. Tanaka, M. Tomonaga, N. Yamamoto, M. Fujii, Bay 11-7082 inhibits transcription factor NF-kappaB and induces apoptosis of HTLV-I-infected T-cell lines and primary adult T-cell leukemia cells, Blood 100 (2002) 1828–1834.

[68] N. Mori, T. Matsuda, M. Tadano, T. Kinjo, Y. Yamada, K. Tsukasaki, S. Ikeda, Y. Yamasaki, Y. Tanaka, T. Ohta, T. Iwamasa, M. Tomonaga, N. Yamamoto, Apoptosis induced by the histone deacetylase inhibitor FR901228 in human T-cell leukemia virus type 1-infected T-cell lines and primary adult T-cell leukemia cells, J. Virol. 78 (2004) 4582–4590.

[69] G. Liao, M. Zhang, E.W. Harhaj, S.C. Sun, Regulation of the NF-kappaB-inducing kinase by tumor necrosis factor receptor-associated factor 3-induced degradation, J. Biol. Chem. 279 (2004) 26243–26250.

[70] A. Imura, T. Hori, K. Imada, T. Ishikawa, Y. Tanaka, M. Maeda, S. Imamura, T. Uchiyama, The human OX40/gp34 system directly mediates adhesion of activated T cells to vascular endothelial cells, J. Exp. Med. 183 (1996) 2185–2195.

[71] A. Imura, T. Hori, K. Imada, S. Kawamata, Y. Tanaka, S. Imamura, T. Uchiyama, OX40 expressed on fresh leukemic cells from adult T-cell leukemia patients mediates cell adhesion to vascular endothelial cells: implication for the possible involvement of OX40 in leukemic cell infiltration, Blood 89 (1997) 2951–2958.

[72] A. Kunitomi, T. Hori, M. Maeda, T. Uchiyama, OX40 signaling renders adult T-cell leukemia cells resistant to Fas-induced apoptosis, Int. J. Hematol. 76 (2002) 260–266.

[73] A. Imura, T. Hori, K. Imada, S. Kawamata, Y. Tanaka, S. Imamura, T. Uchiyama, OX40 expressed on fresh leukemic cells from adult T-cell leukemia patients mediates cell adhesion to vascular endothelial cells: implication for the possible involvement of OX40 in leukemic cell infiltration, Blood 89 (1997) 2951–2958.

[74] M. Takeshita, M. Akamatsu, K. Ohshima, S. Kobari, M. Kikuchi, J. Suzumiya, N. Uike, T. Okamura, CD30 (Ki-1) expression in adult T-cell leukaemia/lymphoma is associated with distinctive immunohistological and clinical characteristics, Histopathology 26 (1995) 539–546.

[75] R. Nasr, A. Rosenwald, M.E. El-Sabban, B. Arnulf, P. Zalloua, Y. Lepelletier, F. Bex, O. Hermine, L. Staudt, H. de The, A. Bazarbachi, Arsenic/interferon specifically reverses 2 distinct gene networks critical for the survival of HTLV-1-infected leukemic cells, Blood 101 (2003) 4576–4582.

[76] G.Q. Chen, J. Zhu, X.G. Shi, J.H. Ni, H.J. Zhong, G.Y. Si, X.L. Jin, W. Tang, X.S. Li, S.M. Xong, Z.X. Shen, G.L. Sun, J. Ma, P. Zhang, T.D. Zhang, C. Gazin, T. Naoe, S.J. Chen, Z.Y. Wang, Z. Chen, In vitro studies on cellular and molecular mechanisms of arsenic trioxide (As_2O_3) in the treatment of acute promyelocytic leukemia: As_2O_3 induces NB4 cell apoptosis with downregulation of Bcl-2 expression and modulation of PML-RAR alpha/PML proteins, Blood 88 (1996) 1052–1061.

[77] I. Ora, L. Bondesson, C. Jonsson, J. Ljungberg, I. Porn-Ares, S. Garwicz, S. Pahlman, Arsenic trioxide inhibits neuroblastoma growth in vivo and promotes apoptotic cell death in vitro, Biochem. Biophys. Res. Commun. 277 (2000) 179–185.

[78] G. Baj, A. Arnulfo, S. Deaglio, R. Mallone, A. Vigone, M.G. De Cesaris, N. Surico, F. Malavasi, E. Ferrero, Arsenic trioxide and breast cancer: analysis of the apoptotic, differentiative and immunomodulatory effects, Breast Cancer Res. Treat. 73 (2002) 61–73.

[79] W.H. Park, Y.H. Cho, C.W. Jung, J.O. Park, K. Kim, Y.K. Im, M.H. Lee, W.K. Kang, K. Park, Arsenic trioxide inhibits the growth of A498 renal cell carcinoma cells via cell cycle arrest or apoptosis, Biochem. Biophys. Res. Commun. 300 (2003) 230–235.

[80] W.H. Park, J.G. Seol, E.S. Kim, J.M. Hyun, C.W. Jung, C.C. Lee, B.K. Kim, Y.Y. Lee, Arsenic trioxide-mediated growth inhibition in MC/CAR myeloma cells via cell cycle arrest in association with induction of cyclin-dependent kinase inhibitor, p21, and apoptosis, Cancer Res. 60 (2000) 3065–3071.

[81] L. Michel, A. Dupuy, F. Jean-Louis, A. Sors, J. Poupon, M. Viguier, P. Musette, L. Dubertret, L. Degos, H. Dombret, H. Bachelez, Arsenic trioxide induces apoptosis of cutaneous T cell lymphoma cells: evidence for a partially caspase-independent pathway and potentiation by ascorbic acid (vitamin C), J. Invest. Dermatol. 121 (2003) 881–893.

[82] S. Mathas, A. Lietz, M. Janz, M. Hinz, F. Jundt, C. Scheidereit, K. Bommert, B. Dorken, Inhibition of NF-kappaB essentially contributes to arsenic-induced apoptosis, Blood 102 (2003) 1028–1034.

[83] R. Nimmanapalli, P. Bali, E. O'Bryan, L. Fuino, F. Guo, J. Wu, P. Houghton, K. Bhalla, Arsenic trioxide inhibits translation of mRNA of bcr-abl, resulting in attenuation of Bcr-Abl levels and apoptosis of human leukemia cells, Cancer Res. 63 (2003) 7950–7958.

[84] V.N. Ivanov, T.K. Hei, Arsenite sensitizes human melanomas to apoptosis via tumor necrosis factor alpha-mediated pathway, J. Biol. Chem. 279 (2004) 22747–22758.